Jianzhong Ge, Shenyang Shi, Jie Liu, Yi Xu, Changsheng Chen,
Richard Bellerby, Pingxing Ding. 2020.
Interannual Variabilities of Nutrients and Phytoplankton off
the Changjiang Estuary in Response to Changing River Inputs.
JGR Oceans. 125(3): e2019JC015

The article has been published at
https://doi.org/10.1029/2019JC015595
by American Geophysical Union.

JGR Oceans

RESEARCH ARTICLE
10.1029/2019JC015595

Key Points:
- Physical and biogeochemical models have been coupled to study pelagic planktonic ecosystem variability in a river estuary system
- Consequences of changing nutrient fluxes over the last 18 years into the estuary on nutrient biogeochemistry and plankton were studied
- Pelagic ecosystem responded rapidly to river discharge and nutrient flux but exhibited different patterns for nutrients and phytoplankton

Supporting Information:
- Supporting Information S1

Correspondence to:
J. Ge,
jzge@sklec.ecnu.edu.cn

Citation:
Ge, J., Shi, S., Liu, J., Xu, Y., Chen, C., Bellerby, R., & Ding, P. (2020). Interannual variabilities of nutrients and phytoplankton off the changjiang estuary in response to changing river inputs. *Journal of Geophysical Research: Oceans*, *125*, e2019JC015595. https://doi.org/10.1029/2019JC015595

Received 26 AUG 2019
Accepted 10 FEB 2020
Accepted article online 12 FEB 2020

Interannual Variabilities of Nutrients and Phytoplankton off the Changjiang Estuary in Response to Changing River Inputs

Jianzhong Ge[1,2], Shenyang Shi[1], Jie Liu[3,4], Yi Xu[1], Changsheng Chen[5], Richard Bellerby[1,4], and Pingxing Ding[1]

[1]State Key Laboratory of Estuarine and Coastal Research, East China Normal University, Shanghai, China, [2]Institute of Eco-Chongming, Shanghai, China, [3]Department of Biological Sciences, University of Bergen, Bergen, Norway, [4]Norwegian Institute for Water Research, Bergen, Norway, [5]School for Marine Science and Technology, University of Massachusetts Dartmouth, New Bedford, MA, USA

Abstract Coastal ecosystems are strongly influenced by terrestrial inputs of freshwater, sediments, and nutrients, particularly in a megariver estuary of the Changjiang River. A remarkable increase in nutrient loading from the Changjiang River to the shelf has been observed over the period from 1999 to 2016 and turned the region into a high eutrophication condition. The Finite-Volume Community Ocean Model and the European Regional Seas Ecosystem Model were coupled to assess the impact of the nutrient loading on the interannual variability of nutrients and phytoplankton. The model was first validated via observational data, and then dynamical analysis were conducted. Singular vector decomposition analysis indicated that the rapid change of local ecosystem was highly correlated with the change in river nutrient contributions. The Changjiang estuarine ecosystem was phosphate limited. The phosphate exhibited local variation, while the abundant nitrate from the river was diluted by the low-nitrate oceanic water. The suspended sediment was significantly correlated with phytoplankton but not with nutrients. The ratio of diatom biomass to dinoflagellate biomass respected a rapid response to strong oscillations in the river nutrient input. High diatom primary production occurred near the sediment front, whereas the dinoflagellate bloom extended significantly offshore. The spring diatom and dinoflagellate blooms had major peaks in the empirical orthogonal function Modes 1 and 2, and the autumn bloom is characterized by secondary peaks from Mode 2 in the autumn.

Plain Language Summary There was an increase in the nutrient input into the Changjiang Estuary with an increased use of agricultural fertilizer as food demand rises globally. Further, there will be additional changes to river and estuary fluxes due to global anthropogenic activities in the future. This study presented the results of a novel coupled physical-biogeochemical model which was designed to examine the seasonal and interannual variability of nutrients and phytoplankton dynamics in the Changjiang Estuary over the period of 1999–2016. The variations of nutrient source from the Changjiang Estuary in the last 18 years had been identified. The model demonstrated that this estuary ecosystem had a rapid response to the changes in riverine nutrients. The total nutrient concentrations, as well as their fluxes of the system, had similar variation patterns with river discharge, indicating that the river was the principal source of nutrients for the nearshore and offshore regions in that area. The phytoplankton population in terms of the ratio between diatoms and dinoflagellates responded quickly to changes in river nutrient fluxes.

1. Introduction

Estuaries are very complex coastal systems that are characterized by strongly nonlinear physical processes. These processes have the significant influences on biogeochemical and ecosystem dynamics in these regions. The terrestrial materials from megariver systems provide abundant dissolved or particulate organic and inorganic matter to coastal and estuarine regions, which can be carried offshore as far as the continental shelf (Milliman & Farnsworth, 2011). Estuaries therefore experience the joint effects of local and remote forcing which leads to complex biogeochemical variability and ecosystem responses.

Nutrient inputs from land (including rivers) into estuaries have greatly increased through, predominantly, anthropogenic activities (Oviatt et al., 2017; Ram et al., 2014; Statham, 2012; Uncles et al., 2003). The major sources of anthropogenic nutrients are untreated sewage (Ram et al., 2014) and agricultural and industrial

discharge. Most of these nutrients enter the river catchments before being transported into estuaries and, often, to the sea. Nitrogen (N), phosphorus (P), and silicate (Si) are the three major nutrients, and among those, the concentrations of N and P have increased dramatically in river systems and associated estuaries due to human impacts (Li et al., 2007; Zhang et al., 1999). N, P, and Si transports from rivers to estuarine and coastal regions doubled from 1952 to 2002 (Mackenzie et al., 2002). As well as increased total nutrient fluxes, relative nutrient ratios and cycling characteristics are also directly influenced by human activity. Silicate concentrations have remained relatively stable in natural river systems. However, exceptions have been observed following hydrological perturbations in upper river catchments such as damming and water diversion for irrigation (Ragueneau et al., 2006). Subsequently, ratios of Si:N:P have been significantly modified in many major estuarine ecosystems (Statham, 2012) and ecosystem impacts have been observed, such as harmful algal blooms and hypoxia (Bianchi et al., 2000; Li et al., 2007; Zhang et al., 2007; Zhou et al., 2008; Zhou et al., 2017; Zhu et al., 2014).

Rivers also transport abundant sediment to coastal areas amounting to 20 billion tons of particulate materials, (Milliman & Farnsworth, 2011) which greatly modulates coastal and oceanic ecosystems. However, due to damming and other human activities, major river systems have suffered significant decreases in sediment input in recent decades (Milliman & Farnsworth, 2011), including the Nile (98%), the Indus (94%), the Mississippi (69%), and the Changjiang (66%) Rivers (CR), as well as smaller rivers such as the Rhone (Giosan et al., 2014; Luan et al., 2016; Yang et al., 2015).

Increasing nutrient input and decreasing sediment load are likely to affect the biogeochemical dynamics of estuarine ecosystems, across multiple temporal and spatial scales. Previous studies identified changes in phytoplankton, zooplankton, and fish populations associated with nutrient variation in global rivers, estuaries, and even large-scale oceans (Hou et al., 2016; Li et al., 2016; Tian et al., 2015; Wang, Chen, et al., 2017; Wang, Wu, et al., 2017; Zhou et al., 2017; Zhu et al., 2009). However, these studies were mainly based on limited observations of nutrient biogeochemistry and have been few studies that were based on detailed spatial and temporal variability in nutrients and phytoplankton so far. Therefore, the main motivation of this work is to figure out how estuarine biogeochemical dynamics respond to the changes in river nutrient and sediment loads over time caused by human activities. We aim to quantify the variations in nutrients and phytoplankton in Changjiang Estuary and to identify the underlying mechanisms which contribute to the observed changes in biogeochemistry, with the application of coupled biogeochemical and physical numerical models.

The mega high-turbidity Changjiang (Yangtze) Estuary was selected to determine interannual variations in nutrients and phytoplankton under the influence significant changes in fluvial nutrient and sediment loads. A novel aspect of this study was that a comprehensive simulated system, combining surface waves and sediment transport and their effects on biogeochemical processes, has been used to resolve physical-biogeochemical interactions in both estuarine and offshore regions, where complex dynamics between sediments, nutrients, and phytoplankton occur.

This paper is organized as follows. The study area of Changjiang Estuary, observation data, and numerical model are described in section 2, followed by a description of the variations in freshwater discharge, nutrient concentrations, and sediment load in the upstream Changjiang River observed over the last two decades. Subsequently, in section 4, the coupled model used in this study is described and validated. Seasonal and interannual variations in nutrient concentration and phytoplankton populations in the offshore region of the estuary are then described in sections 5 and 6, respectively. Finally, the conclusion is given in section 7.

2. Materials and Methods

2.1. Study Area

The CR is the largest river in the Asia, and it transports abundant freshwater and sediment to the shelf of the East China Sea (ECS), producing an extensive estuarine region (Figure 1). The CR contributed an average annual freshwater volume of 896 km^3 and sediment load of 390 Mt into the estuary over periods of 1950–2010 (CWRC (Changjiang Water Resources Commission), 2011). These flux rates were measured at Datong hydrological gauge station, the nearest hydrological station to the Changjiang Estuary, which is located about 620 km upstream from the ECS. The CR has shown a continuous increase in nutrient content since the 1950s, with even larger increases observed after 1980s (Chen et al., 2003), following increasing

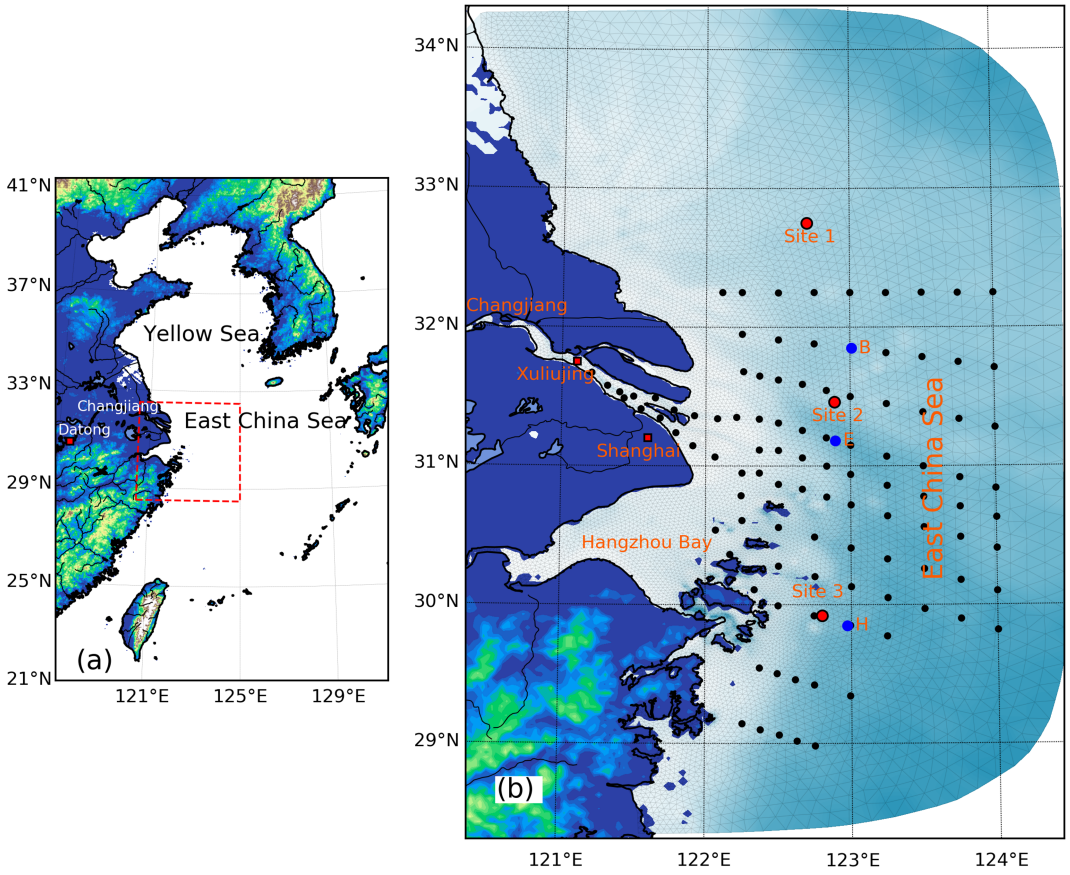

Figure 1. The position of the Changjiang River, Changjiang Estuary (dashed rectangle) and adjacent coastal region (a) and unstructured mesh for the coastal model for the Changjiang Estuary (b). Three individual locations (Sites 1, 2, and 3) from north to south offshore region were included for further analysis. Black dots indicate the historical survey sites from 2013 to 2016. Among them, three blue dots of Sites B, E, and H indicate selected observational sites for time series model validation.

agricultural application of chemical fertilizers (Li et al., 2007). Coastal phytoplankton populations have exhibited community change with earlier diatom dominance weakened in favor of increasing contributions of dinoflagellates (Zhou et al., 2008). Zhou et al. (2008) and Zhu et al. (2014) suggested that the dominance shift was mainly caused by an increase in nitrogen and phosphate concentrations and a decrease in silicate concentration.

2.2. Data

Freshwater discharge, sediment load, and nutrient concentrations data, collected at the Datong station (red dot in Figure 1a) from 1999 to 2016, were used in this study. Freshwater discharge was sampled daily, and monthly averaged sediment concentration and total load were recorded. Concentrations of nitrate, phosphate, silicate, and ammonia were also collected, although they were recorded at a lower sampling frequency than river runoff and sediment. These nutrient data came from various sources based on field measurements from the Datong station and from observations downstream to the Shelf from 1999 to 2014 (Dai et al., 2011; Gao et al., 2012; Zhu et al., 2014).

Historical observations from surface, middle, and bottom layers of the estuary and shelf for the period from 2013 to 2016, with a sampling frequency of twice per year of temperature, salinity, dissolved nutrient concentrations (DIN, DIP, and DSi), and *Chlorophyll a* (*Chl a*) at 92 sites (blue dots in Figure 1b) around the Changjiang Estuary and adjacent regions, were also applied in this study. The most upstream site Xuliujing (in Figure 1b) was defined as the river source following Gao et al. (2012), who confirmed that the Changjiang freshwater from Datong station was well represented by samples from Xuliujing site. From these biannual surveys, it was not possible to characterize interannual physical-biogeochemical and

ecosystem variability in the offshore estuarine system. However, these data provided a comprehensive data set to calibrate and test the physical and biogeochemical modeling system.

2.3. Numerical Model

A coupled modeling system had been applied to examine the controlling mechanism for interannual variations under high-turbidity sediment suspension in and off Changjiang Estuary. In order to consider the physical and biogeochemical dynamics and their interactions in this system, multiple models had been integrated. The physical system was represented through the Finite-Volume Community Ocean Model (FVCOM), which provided two-domain nesting hydrodynamics for the regional and coastal oceans. The ECS and its connected oceans were covered by basin-scale unstructured triangular mesh (Figure 5a in Ge et al., 2013). Through the common-grid nesting method (Ge et al., 2013), the shelf-scale model was nested into the coastal FVCOM model for the Changjiang Estuary. Sediment dynamics were represented using the community sediment transport model FVCOM-SED, which has been fully validated with cohesive sediment dynamics (Ge, Shen, et al., 2015). The generation, breakdown, and propagation of surface waves were simulated using FVCOM-SWAVE (Qi et al., 2009). These three models combined wave-current-sediment interactions as proposed in Wu et al. (2011). Accurate geometric fitting for the irregular coastlines and islands and arbitrary local mesh refinement around large slope gradients, FVCOM, could provide precise numerical calculations to ensure mass and momentum conservation, which is crucial for a long-term integration from years to decades.

Nutrient biogeochemistry and planktonic ecosystem dynamics were simulated using the European Regional Seas Ecosystem Model (ERSEM ver. 15.06), which is a generic and well-established biogeochemical cycling model used to describe lower trophic levels of marine food webs (Butenschön et al., 2016). This model integrates essential components of the pelagic and benthic dynamics of marine ecosystems and incorporates important biogeochemical processes such as primary production, predator dynamics, and decomposition of organic material by heterotrophic bacteria. In our setup, ERSEM classified phytoplankton into picophytoplankton (<2 μm), nanophytoplankton (2–20 μm), microphytoplankton (>20 μm), and diatoms based on their individual trait size. ERSEM model is a comprehensive ecosystem model which includes most biogeochemical processes of organic/inorganic, dissolved/particulate, and pelagic/benthic system.

While ERSEM considers both dissolved and particulate inorganic/organic matter, these refer to autochthonous compounds and not external/forced fluxes. The nonliving organic matter in ERSEM contains labile dissolved organic matter, semilabile organic matter, semirefractory organic matter, small particulate organic matter, medium size particulate organic matter and large particulate organic matter. The full dynamics associated with these pools, which include particulate organic matter for nitrogen, phosphate, and silicate, were described by Butenschön et al. (2016). In this study, these components were fully included in the model simulation.

Coupling of the physical FVCOM and biogeochemical ERSEM was accomplished using the Framework for Aquatic Biogeochemical Models (FABM), which is a Fortran-based programming framework, designed to couple models of marine and freshwater systems (Bruggeman & Bolding, 2014). It provides a complete, efficient, and flexible application program interface that can be easily attached to various models. In this study, FABM was used to link physical variables of the FVCOM model, including temperature, salinity, light, vertical velocity, suspended sediment, and concentration, with ERSEM. The ERSEM model then incorporated these physical variables into a biogeochemical calculation and returned values for salinity to the FVCOM model. FVCOM was also used to model physical advection, diffusion, and time integration. All biogeochemical variables and their concentration and rates for ERSEM were processed by FABM, which are provided in the supporting information S1.

The model grid for the Changjiang Estuary and its adjacent region consisted of an unstructured triangular mesh (Figure 1b). The upstream boundary was located at the Datong gauge station, and lateral open boundary was placed at 124.5°E. The north and south lateral boundaries were extended to 34.2°N and 28.25°N, respectively, with the purpose of reducing the numerical interference from the remote boundary in our interested estuarine region.

In order to represent the response of nutrients and phytoplankton to anthropogenic and natural changes over the last 18 years, the model simulation covered the period from 1 January 1999 to 31 December 2016.

The upstream river boundary was driven and determined by daily freshwater and sediment discharge collected at Datong station. The seasonal nutrient concentrations measurements were considered to represent nutrient discharge. The physical conditions of the lateral boundaries of the model were nested from the large-scale FVCOM to ECS and connected oceans (Ge et al., 2013), which provided both astronomical tides and ocean circulation. Ocean surface forcing, including surface wind at 10 m height, shortwave, longwave, latent, and sensible radiation flux, was provided by the ERA Interim data set using 6 hr intervals. Sea surface temperature (SST) was assimilated with remote sensing data to provide accurate water temperature simulation. Data from the Advanced Very High-Resolution Radiometer L4 for 1999 to 2004 and GHRSST/JPL for 2005–2016 were applied in the SST assimilation.

2.4. Methods

The anomaly analysis was used in this study to determine the fluctuation of a derived time series for a specific time window. The mean background value for physics and biogeochemistry was determined by averaging observational data over the study period in this study. Monthly anomaly was then calculated subtracting observed or simulated monthly results from background values.

Singular value decomposition (SVD) was also applied to identify significant spatial correlations between pairs of physical/biological components, as well as their temporal variation of principle components (expansion coefficients) (Bjornsson & Venegas, 1997).

3. Changes in River Discharge, Sediment, and Nutrients

3.1. Freshwater Discharge

There were clear seasonal variations in the monthly averages of Changjiang freshwater discharge from 1999 to 2016 (Figure 2a), with a maximum of 48,412; 10,792 m^3/s reached in July and a minimum of 13,228 $m^3/s \pm$ 3,746 m^3/s in January. The annual freshwater flux climatology was calculated (black curve in Figure 2b), showing that large interannual variability has occurred over the 18 years under investigation (Figure 2b). The low freshwater loads were observed in the years 2006 and 2011, while the highs were documented for the years 2010 and 2012.

3.2. Sediment

In contrast to the relatively constant annual discharge of freshwater, the sediment load of the CR decreased over the last 18 years from a peak of 370 Mt in 2000, which was close to the calculated mean value across 1950–2010 (Luan et al., 2016), declining to around 100 Mt by 2006 and modulating between 200 and 100 Mt up in 2016 (blue curve in Figure 2b). The changes in sediment loads into the estuary were primarily caused by the water-sediment regulation scheme of the Three Gorges Dam in the upstream CR in 2003 (Luan et al., 2016; Yang et al., 2015). Sediment concentrations measured at Datong station decreased from >0.5 g/L in the summer of 2000 to ~0.15 g/L in the summers of 2015 and 2016 (Figure 2c). A similar pattern also occurred in autumn, while no observable trend could be seen in spring and winter

3.3. Nutrients

Nutrient concentrations measured at Datong station during 1999–2017 were shown in Figure 3. Large increases in the concentrations of nitrate and dissolved inorganic phosphorus (DIP) can be observed during this period (Figures 3a and 3b), with lower increases for dissolved silicon (DSi) and ammonia ions (Figures 3c and 3d). The trends in DIN and DIP were significant with $P < 0.001$. Their increase had been kept for several decades due to human activities (Li et al., 2016; Wang, 2006), which remains in this study period. There were no significant trends showed for DSi ($P > 0.2$) and ammonia ($P > 0.5$) respectively, indicating that these two nutrient concentrations did not show significant trend from 1999 to 2016. Previous observations in the downstream sites also confirmed a relatively stable value in DSi in recent decades, under the circumstances that sediment load in the CR was decreasing but dissolved silicate was still oversaturated (Gao et al., 2012). Additionally, Chetelat et al. (2008) and Gaillardet et al. (1999) suggest that strong decrease of sediment load did not lead to significant weathering rates of silicate rocks. Therefore, the decreased sediment contents did not strongly change the equilibrium between silicate rocks and the dissolved silicate in the riverine waters (Gao et al., 2012).

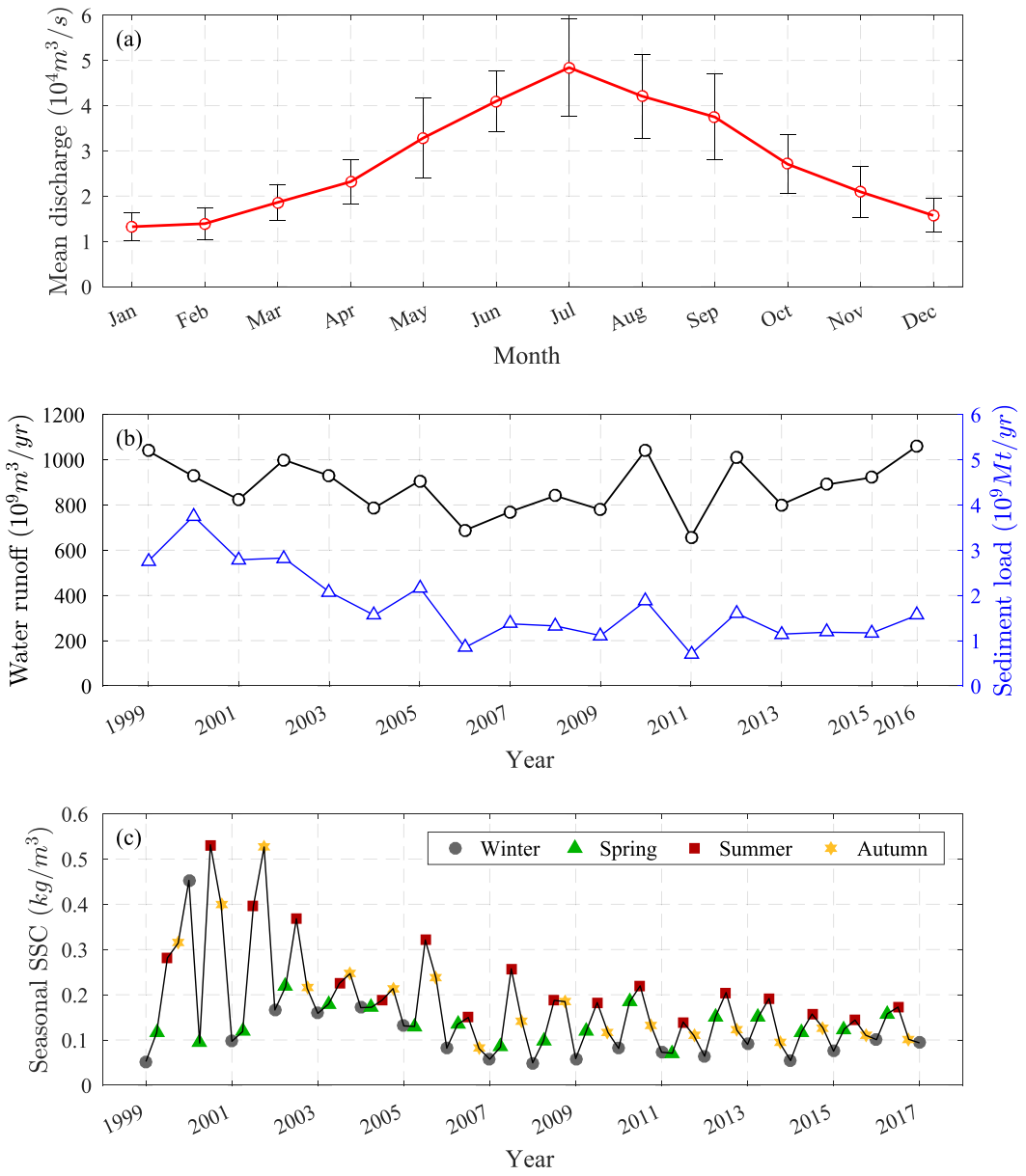

Figure 2. The monthly averaged freshwater discharge rate and its standard deviation (a), annual water runoff and sediment load (b), and seasonally averaged suspended sediment concentration (c) during 1999–2016.

Based on calculations of nutrient concentration, the Si/N and Si/P ratio dropped from ~0.96 to 0.75 and from ~103.7 to ~57.5, respectively from 1999 to 2016. These ratio declines indicated a substantial shift in the nutrient structure of the estuary over the past two decades. Such a shift may have contributed to phytoplankton community changes in the Changjiang Estuary and the inner shelf of ECS, resulting in an increase of dinoflagellates and an associated decrease of diatom abundance (Jiang et al., 2010; Zhou et al., 2008).

4. Model Validation

4.1. Time Series Comparison at Selected Sites

Three offshore sites, Site B (123.0092°E, 31.8480°N), Site E (122.8960°E, 31.1820°N), and Site H (122.9734°E, 29.8539°N) (Figure 1b), were selected to explore time series comparisons between observed and modeled results. These three sites, showed in Figure 1b, were all located in offshore regions with a longitude of about 123.0°E, and their latitudes cover the north, middle, and south regions. The model-data comparisons for

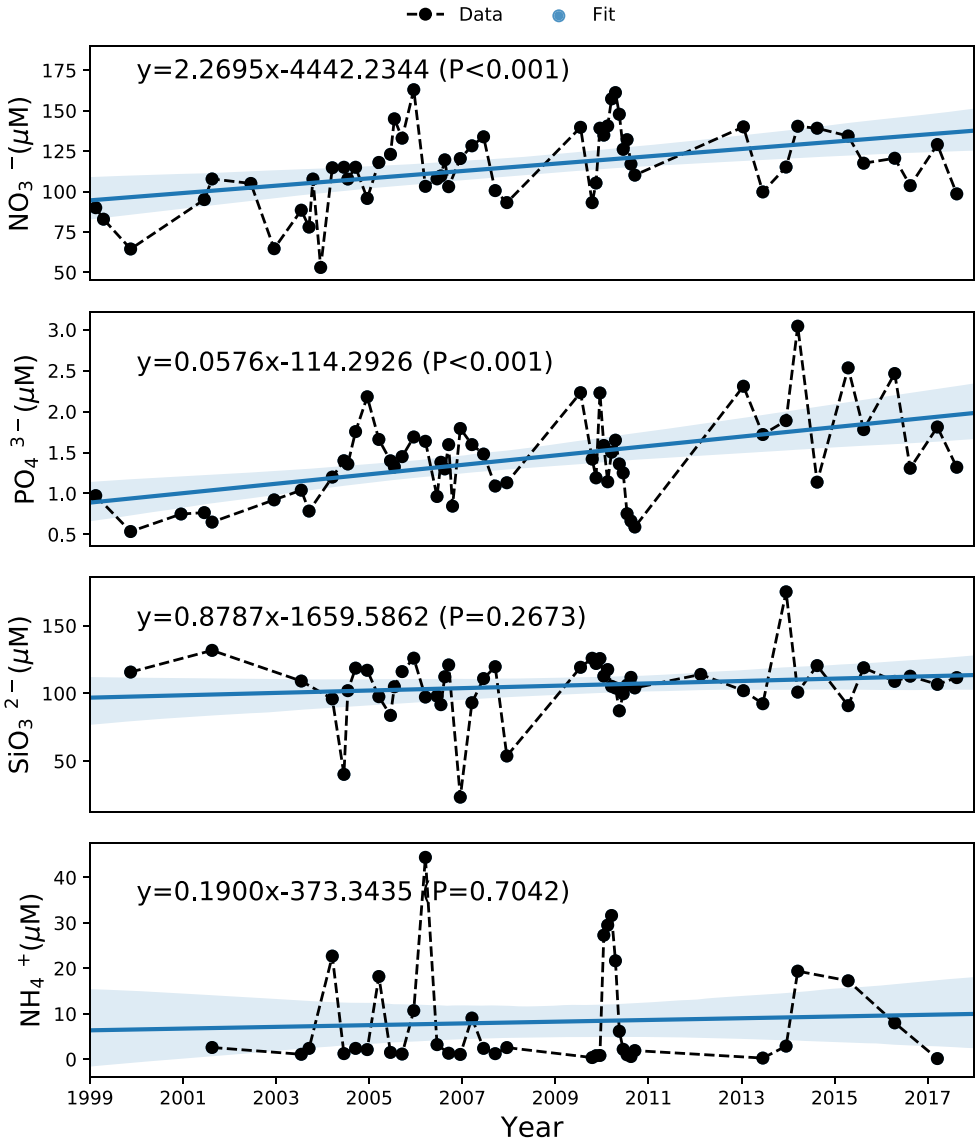

Figure 3. The concentration of nitrate (a), phosphate (b), silicate (c), and ammonia (d) observed at the Datong station from 1999 to 2017. The solid and dashed lines indicate linear regression relation and its 95% confidence level. The regression equations were included in the corresponding panels.

surface temperature, salinity, DIN, DIP, and *Chl a* are showed in Figure 4. The model provided reasonable simulations of temperature and salinity from the north to the south over the duration of the survey (Figures 4a–4f). The variations in nutrient concentrations across 2013–2016 were also nicely captured. DIN had strong annual oscillations at all three sites (Figures 4g–4i), due to significant variations of concentrations in river sources and discharge rates (Figures 2b and 3). This variation pattern indicated DIN was a sufficient nutrient factor in the biogeochemical cycle. In contrast, the DIP showed a more regular periodic variation at these three sites (Figures 4j–4l). The model matched the observed changes in DIP and DIN closely, indicating that the model system performed well at characterizing offshore nutrient dynamics. The model also revealed the main patterns of the *Chl a* concentration at these three sites (Figure 4m–4o).

4.2. Overall Quantification of Modeling Results

The model results were validated by the time series of the model-data comparison at specific locations. However, it was unable to provide an overall estimation of model accuracy for whole region, from the low-

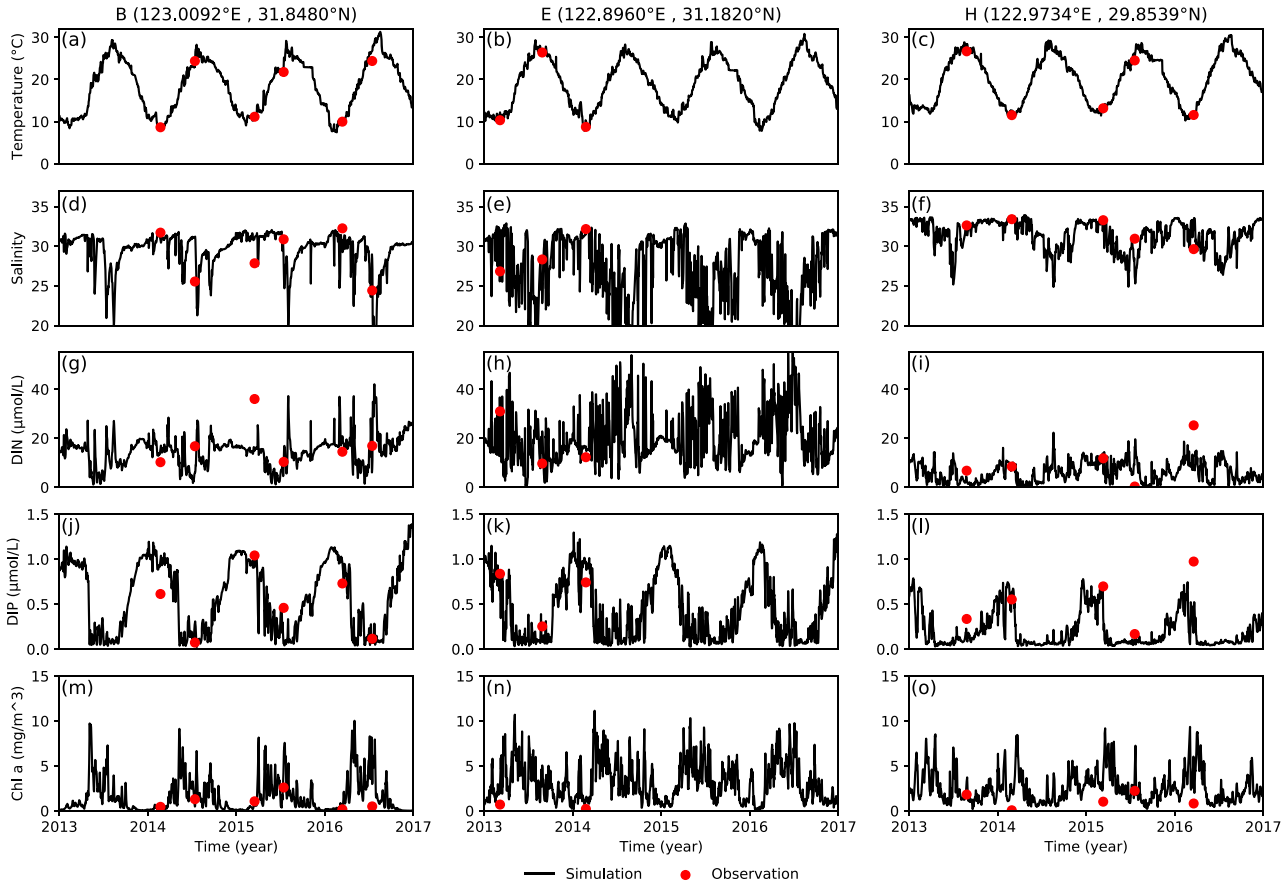

Figure 4. Model-data comparison for temperature (a–c), salinity (d–f), DIN (g–i), DIP (j–l), and *Chl a* (m–o) at selected Sites B (left column), E (middle column), and H (right column).

salinity/high-SSC nearshore region to the high-salinity/low-SSC offshore region. A Taylor diagram approach was used to quantify model performance over the whole computational domain for all relevant physical and biogeochemical variables (Figure 5). The measured data from all survey sites in Figure 1b, including salinity, temperature, nitrate, phosphate, silicate and *Chl a*, were all used to make the overall quantification. Annual sample numbers ranged from 310 in 2013 to 716 in 2016. Spatial and temporal interpolations from model results were applied to the sampling sites over time. All model-data comparisons from these samples were used to determine the statistics of the Taylor diagram. The correlation coefficient R for salinity was >0.8, except for 2015, and >0.95 for temperature (Figures 5a and 5b), indicating that the FVCOM-ERSEM model system was capable of accurately replicating the physical processes of the estuary. The correlation coefficients for all nutrients, including DIP, DIN, and DSi, were all greater than 0.4, and most of them were around 0.8. The standard deviation (SD) of the model simulation was greater than all observed values for nutrients, except for the results in 2013, which had a smaller SD (Figure 5c–5e). The model overestimated *Chl a* concentration. The overall SD for all years was about twice the observed value (Figure 5f). The low skill for the *Chl a* concentration may be due to inadequate observational temporal coverage. Phytoplankton have been observed to exhibit high-frequency oscillation and fast vertical migration even in surface 1 m layer based (Lou & Hu, 2014). Thus, *Chl a* concentration was much more difficult to capture than dissolved nutrients. Additionally, the suboptimal representation of local phytoplankton community was determined by parameterization adopted consistently across the contrasting environments (Butenschön et al., 2016). The root-mean-square difference was less than 5.0 PSU for salinity and 2.5 °C for temperature. The root-mean-square difference for nitrate was <20 μM for all years combined (Figure 5c) and 0.5 μM for phosphate (Figure 5d). More validation results could also be found at Ge et al. (2020).

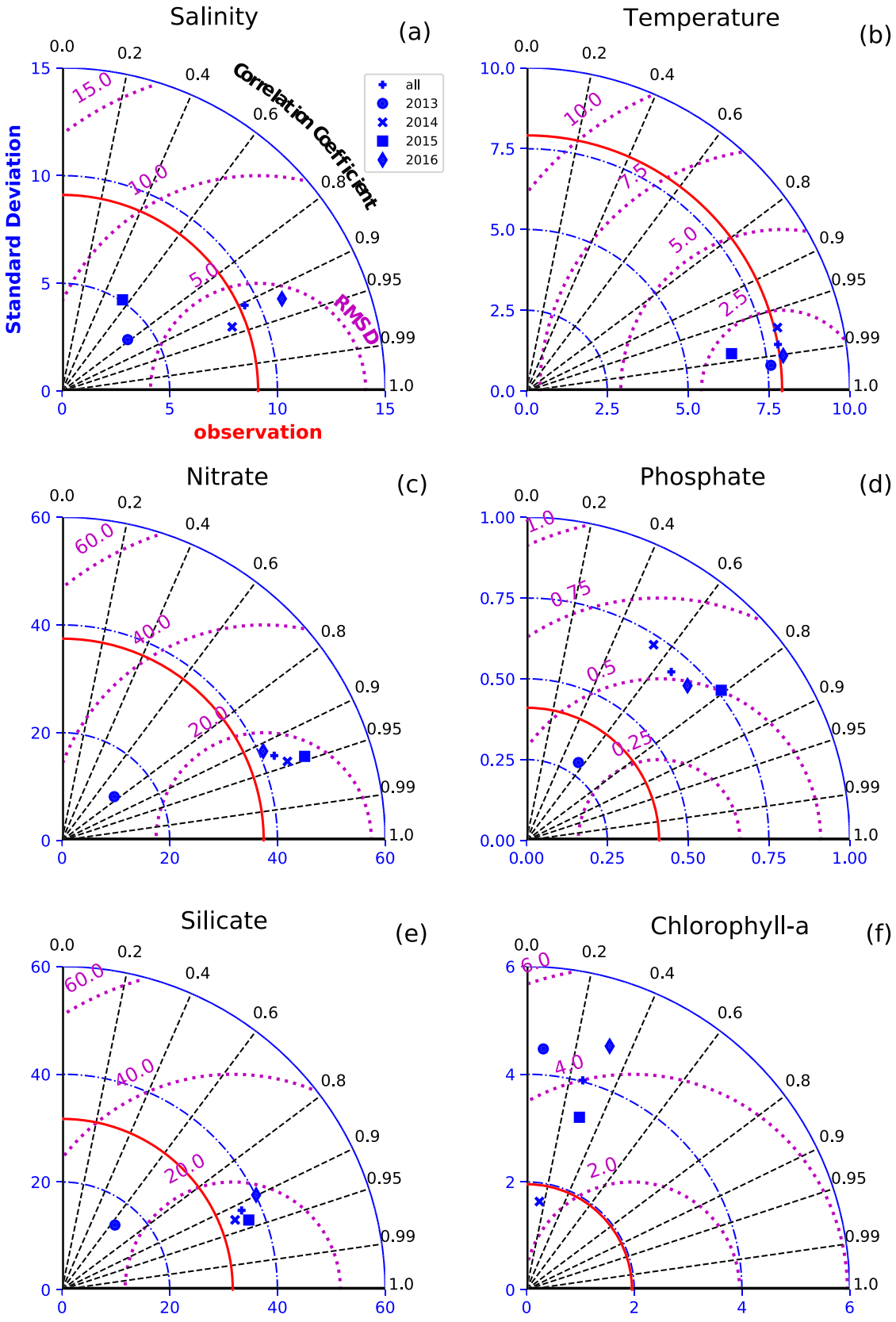

Figure 5. Taylor diagrams for salinity (a), temperature (b), nitrate (c), phosphate (d), silicate, (e), and *Chl a* (f) based on observed values from 90 survey sites from 2013 to 2016 and corresponding model prediction.

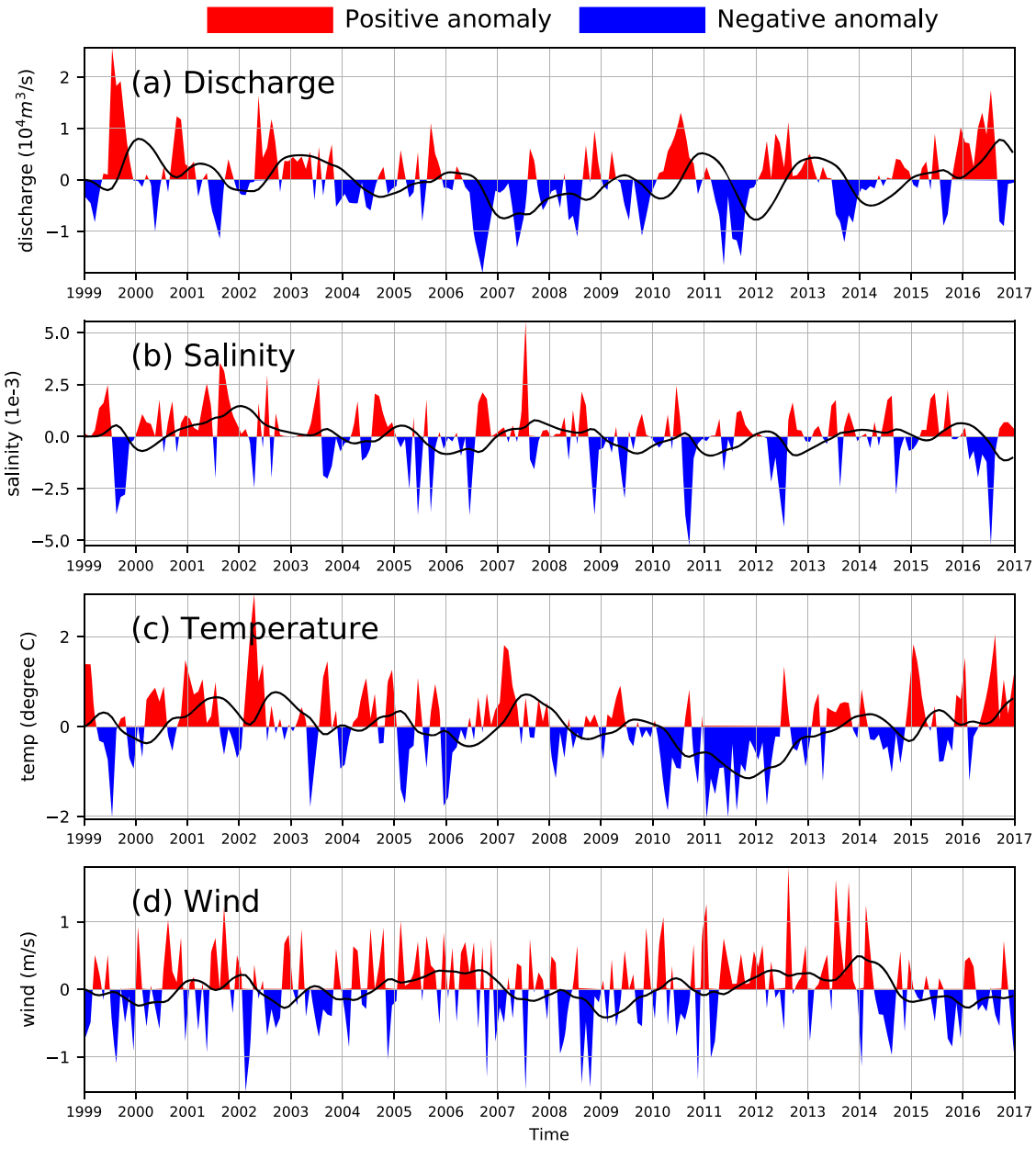

Figure 6. Monthly anomalies and low-pass-filtered interannual trend (black lines) of freshwater discharge rate at Datong station (a), salinity (b), temperature (c), and wind speed (d) at Site 2 from 1999 to 2016.

5. Variability in Physical Processes and Nutrients

5.1. Physical Drivers

Interannual variability in physical drivers at the river mouth (Site 2), including freshwater discharge, salinity, temperature, and surface wind, was calculated using anomaly detection (Figure 6). Interannual trends were determined using a low-pass filter for anomalous signals with a cutoff frequency of 1/24.0 per monthly anomaly. Freshwater discharge showed positive anomalies during 1999–2004, 2011, 2013, and 2016, indicating higher river flux in these years (Figure 6a), especially during the summer. A large negative anomaly was also observed in 2006, when the lowest discharge rate in history was recorded for the CR (Luan et al., 2016). Another negative anomaly occurred in 2011. Since the salinity of the river mouth and the offshore region are both strongly influenced by river discharge, salinity varies with changes in river flux with negative response. These two variables had a negative correlation coefficient R^2 of −0.69 at Site 2 (Figure 6b). The SST

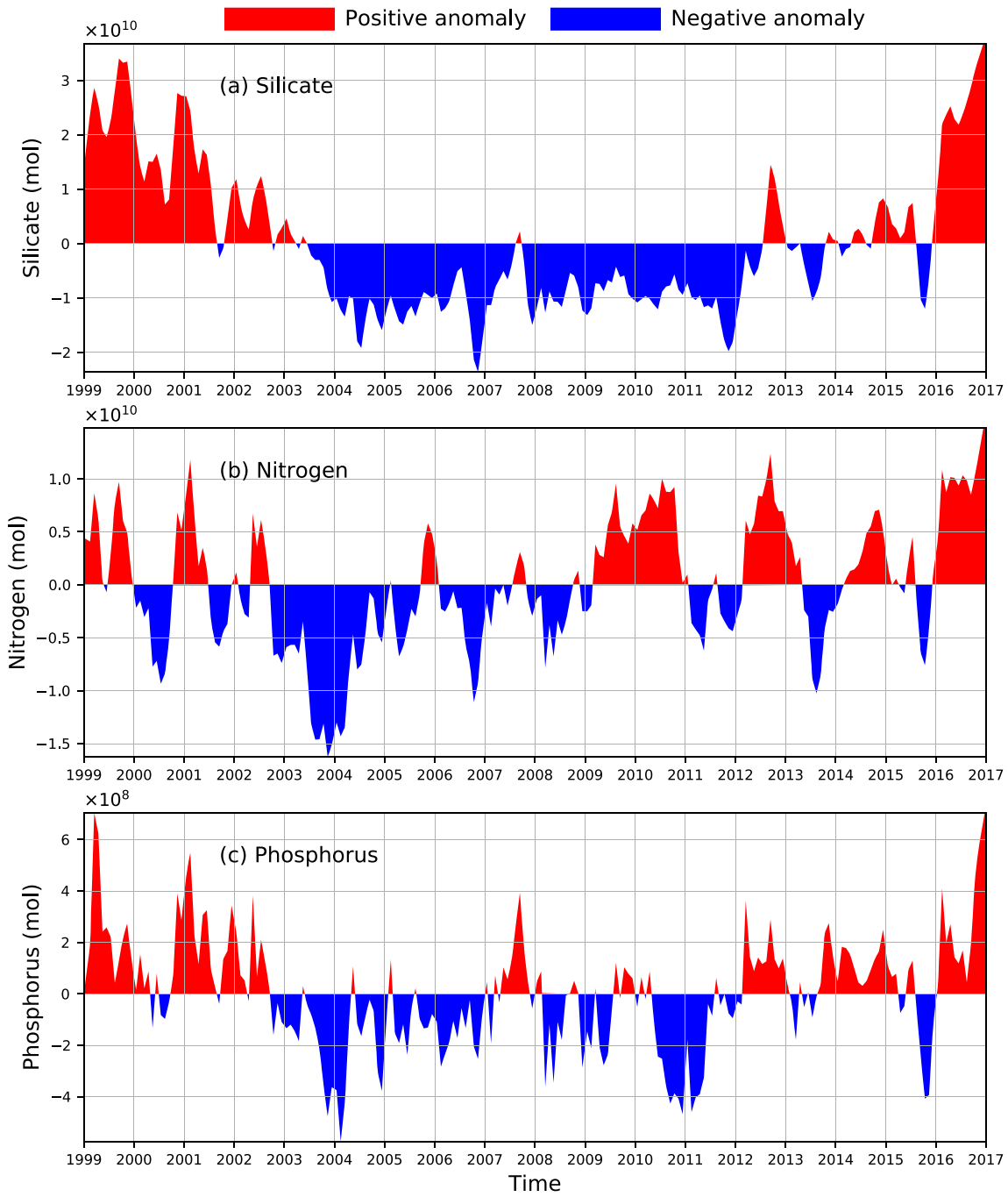

Figure 7. Monthly anomalies and low-pass-filtered interannual trend of total abundance of dissolved inorganic silicate (a), nitrogen (b), and phosphorus (c) in whole computational domain.

anomalies indicated a relatively warm environment before 2004, and in 2007, 2015, and 2017, and colder conditions during 2005, 2006, and 2011–2013 (Figure 6c). The sea surface wind speed displayed weak positive anomalies during 2005–2006 and 2012–2014 (Figure 6d).

5.2. Total Nutrients

To determine variations throughout the entire estuary, anomalies of total nutrients, defined as total abundance of dissolved inorganic silicate (TS), nitrogen (TN), and phosphorus (TP), were integrated across the whole computational domain and water column, as shown in Figure 7. It shown there were great

Table 1
Square Covariance Fractions (SCF), Cumulative SCF (CSCF), and Coupling Correlation Coefficient for Each Leading Mode for SVD (SAL, DIN), SVD (SAL, DIP), SVD (SED, DIN), SVD (SED, DIP), and SVD (SED, CHL)

Mode	SCF	CSCF	*R*	Time scale
SVD (SAL, DIN)-1	84.9%	84.9%	0.87	Seasonal
SVD (SAL, DIN)-2	11.3%	96.2%	0.67	Seasonal/interannual
SVD (SAL, DIP)-1	84.1%	84.1%	0.79	Seasonal
SVD (SAL, DIP)-2	13.5%	97.6%	0.74	Seasonal/interannual
SVD (SED, DIN)-1	58.2%	58.2%	0.61	Seasonal/interannual
SVD (SED, DIN)-2	40.0%	98.2%	0.86	Seasonal/interannual
SVD (SED, DIP)-1	65.3%	65.3%	0.76	Seasonal
SVD (SED, DIP)-2	32.9%	98.2%	0.74	Seasonal
SVD (SED, CHL)-1	79.4%	79.4%	0.86	Seasonal
SVD (SED, CHL)-2	18.8%	98.2%	0.62	Seasonal

Note. The values of *R* were derived from the relationships in both first and second modes in the SVD analysis. The timescale determined from each mode was also included.

variation in the total abundance. Results also revealed the impact of the CR on the nutrient dynamics of the estuary. During periods of higher flux rate (1999–2002, 2012), TS, TN, and TP all demonstrated positive trends (Figures 7a–7c). Total nutrients also show a negative anomaly in the low-flux rate period around 2006. The river flux oscillation pattern was the strongest over 2010–2016. Nutrient concentrations showed corresponding fluctuations in Figure 7.

5.3. Effect of River Nutrient Inputs on Estuarine Nutrient Variability

In the Changjiang Estuary and its adjacent regions, river freshwater discharge has been shown to be the most important factor influencing the salinity. In previous studies on salinity dynamics (Chen et al., 2008; Ge et al., 2013; Ge, Ding, et al., 2015; Wu et al., 2011; Xue et al., 2009), the evaporation and precipitation of water were not included. In view of climatological mean, these two terms are balanced, so they could be neglectable if the long-term variation is considered. The salinity has a conservative nature from nearshore to offshore region. Therefore, estuarine salinity can be used as a marker for the CR's freshwater discharge. Salinity mainly shown an opposite variation behavior against river flux rate, as shown in Figure 6, particularly at some high value of discharge anomalies in 1999, 2006, 2012, and 2016. The calculated linear correlation coefficient R^2 at selected sites ranged from −0.33 at Site 1 to −0.77 at Site 3 with all P values < 0.001, indicating significant negative correlation. To determine the spatial correlation between river flux and offshore nutrient concentration, SVD analysis was conducted on the cross-variance matrix between model-simulated salinity and nitrate from 1999 to 2016, which we classified as SVD (SAL, DIN). Similar analysis was performed to compare salinity and phosphate and was classified as SVD (SAL, DIP).

The square covariance fractions (SCF) and cumulative SCF of the two leading modes of SVD analysis were shown in Table 1. The cumulative SCF is the sum of SCFs of the first, second, and other minor components. The cumulative SCF of the first and second modes for SVD (SAL, DIN) and SVD (SAL, DIP) accounted for 96.2% and 97.6% of their own total square covariance, respectively.

The SVD analysis showed that salinity and nitrate variabilities were well represented by the first and second modes (SVD1 and SVD2), which represented 84.9% and 11.3% of the total variance, respectively (Figures 8a and 8b). The third and fourth modes had weak contributions (<4%) to the total variance, which were not significant. The salinity variance (<0) in SVD (SAL, DIN)-1 essentially represented the influence of the river on the measured nitrate concentrations. The positive variance of nitrate mainly covered the river mouth, Hangzhou Bay and Zhejiang offshore region, which were all situated along the main path of the river's freshwater pathway (Ge, Ding, et al., 2015). Smaller variance in SVD (SAL, DIN)-2 was found off the Jiangsu and Zhejiang coasts (Figure 8b), which indicated a seasonal signal from biological consumption and also the presence of a secondary water source. The Taiwan Warm Current exhibited persistent intrusion along the Zhejiang coasts, reaching the offshore region of the Changjiang Estuary (Chen et al., 2003). This current was the major remote water source carrying salinity, DIC, and nutrients off the Zhejiang coast. Additionally, the Jiangsu Coast Current transports water and nitrate from the northern region of the Yellow Sea to the Jiangsu offshore region (Chen et al., 2008).

The first and second modes of SVD analysis for salinity and DIP accounted for 84.1% and 13.5% of the total variance (Figures 8e and 8f). The correlation coefficients of these leading two modes were 0.79 and 0.74, respectively (Table 1), indicating a strong correlation existing between the two variables. However, the first mode did not show a significant match between salinity and DIP (Figure 8e). This indicated that changes in DIP did not closely correspond with variations in salinity, suggesting that the CR cannot provide adequate DIP to phytoplankton growth in the offshore regions and that phosphate was the limiting factor in the ecosystem. Additionally, the mismatch between salinity and DIP in the first mode may be related with some other physical and biogeochemical processes that were not included in the FVCOM-ERSEM system, such as sediment release/absorption for DIP (Shi et al., 2014; Xu et al., 2013; Yang et al., 2013). The river-contributed DIP covariance pattern matched the covariance of salinity in the second SVD mode,

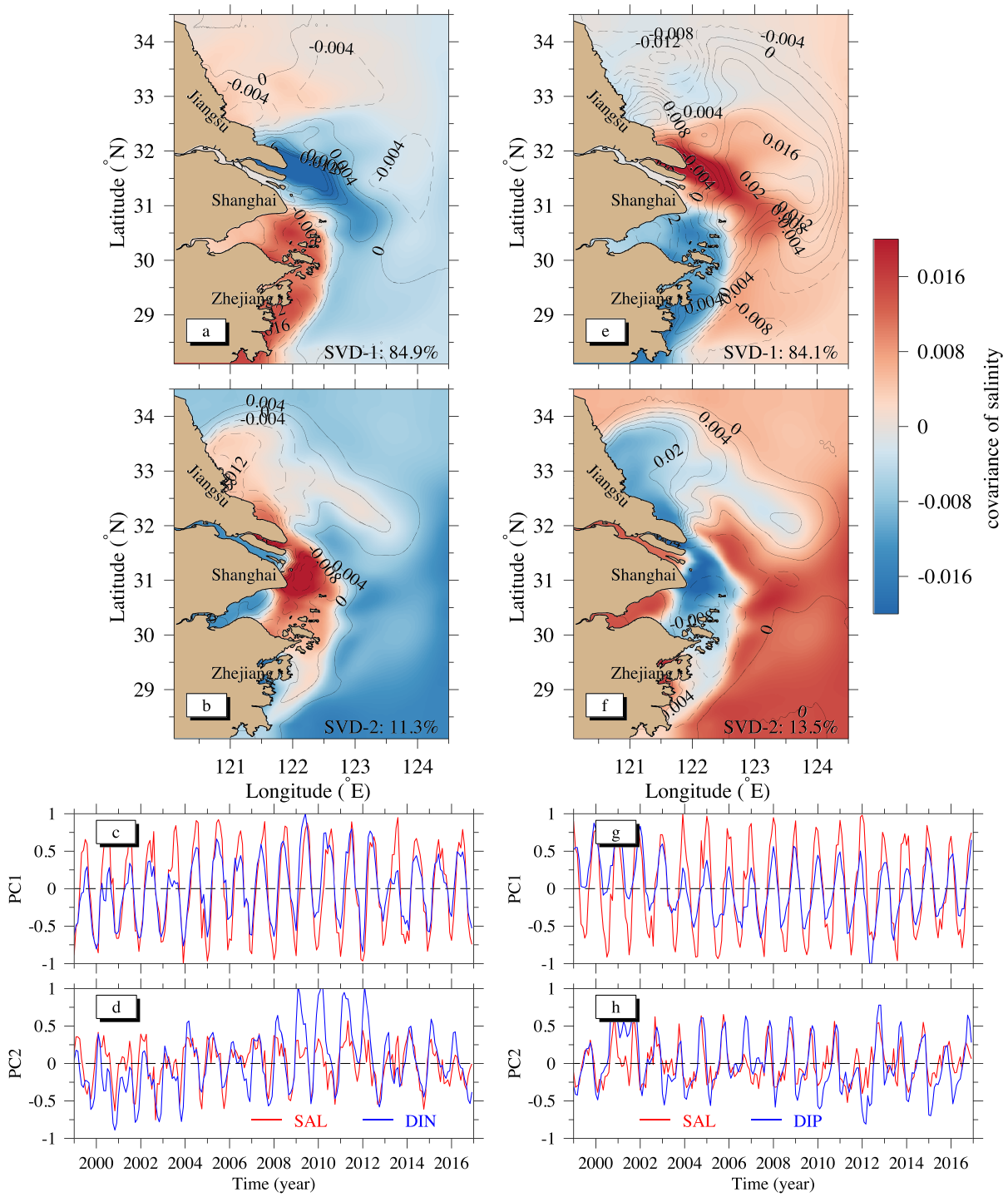

Figure 8. Heterogeneous spatial correlation map of salinity (image) and DIN (contours) for the first (a) and second (b) modes from SVD analysis and their temporal expansion coefficients for first (c) and second (d) modes. And heterogeneous spatial correlation map of salinity (image) and DIP (contours) for the first (e) and second (f) modes from SVD analysis and their temporal expansion coefficients for first (g) and second (h) modes.

especially around the Jiangsu nearshore region and Changjiang Estuary (Figure 8f). Since these regions were always dominated by high-turbidity water, phosphate was not consumed by phytoplankton growth in this area. The area was predominantly a conservative environment for phosphate. Therefore, DIP had a positive correlation with river flux (Figure 8e and 8f). The Zhejiang offshore region, however, was an active

area of phytoplankton growth, which strongly depended on the concentration of dissolved phosphate. The seasonal growth of phytoplankton had a much stronger effect on variation in phosphorus concentration than river discharge. The second mode of SVD (SAL, DIP) indirectly demonstrated the effect of vertical mixing on phosphate variation (Figure 8f). In the nearshore region, salinity was highly related to river discharge. The phosphate showed negative variation against salinity in the river mouth of Changjiang Estuary and positive variation along the Jiangsu nearshore region.

The expansion coefficients for salinity and DIN for the first mode of SVD (SAL, DIN) demonstrated significant annual cycles (Figure 8c), similar with those for SVD (SAL, DIP) (Figure 8g). All major physical forcings, such as river discharge rate, sediment (Figure 2), and temperature, showed clear annual patterns. These dynamics produce strong annual cycles for salinity and nutrients in the estuary in the first SVD mode. Moreover, the second modes of these two SVD analyses also showed significant seasonal cycles (Figures 8d and 8h). However, the expansion coefficients for these second modes were also mixed with interannual signals with varied amplitude. Our results indicated higher expansion coefficients for DIN in the winter from 2009 to 2012 (Figure 8d), and a similar pattern occurred in the expansion coefficients of SVD (SAL, DIP) in the winters of 2006, 2007, 2011, and 2013 (Figure 8h), which matched well with significant negative anomalies in river discharge (Figure 4a). This result suggested that variability in river discharge had a stronger effect on the estuarine DIP process than it did on DIN.

5.4. Effect of Sediment on Nutrients and *Chl a* Variability

Coupled spatial distributions of surface suspended sediment and biogeochemical variables were also identified using the SVD method on paired variables such as sediment and nitrate with label of SVD (SED, DIN), sediment and phosphate with label of SVD (SED, DIP), and sediment and *Chl a* with label of SVD (SED, CHL).

The correlation coefficients of the leading two modes of SVD (SED, DIP) and SVD (SED, DIN) were relatively low (Table 1). The correlation did not exhibit strong variation with changes in sediment signal. Sediment concentration in the Changjiang Estuary is mainly determined by local settling and resuspension (Ge, Shen, et al., 2015). The correlation did not indicate significant river impact. Therefore, the two leading modes for SVD analysis only accounted for 58.2% and 40% of their own total square covariance against the DIN, respectively. Concentrations of sediment and DIN did not show significant spatial correlation, indicating that the variation in DIN did not depend on sediment transport. Therefore, variation in DIN concentration was interpreted to predominantly indicate the process of dilution in the estuary (Figures 9a and 9b).

Comparatively, the result of SVD (SED, DIP) also showed relatively large percentages for its first mode, which was 65.3%. The highest correlation was located in the nearshore areas in the first mode (Figure 9c), suggesting that the decrease in nearshore sediment concentration could indirectly decrease the phosphate concentration, perhaps reflecting lower fluvial phosphate supply and increased autotrophic consumption through increased phytoplankton production. The second mode had 32.9% of the total covariance. The highest spatial correlation occurred mainly in the river mouth and the northwestern offshore region (Figure 9d). This distribution indicated that an increase in sediment concentration suppresses phytoplankton growth, which would decrease the consumption of dissolved phosphate. Since the FVCOM-ERSEM coupling did not include the sediment-induced absorption and desorption dynamics in the biogeochemical model, the match between sediment and DIP occurred in the river mouth and the northwest offshore region was not related to the absorption/desorption under low- and high-salinity environment. But the sediment-induced light attenuation is a key factor that decreases the euphotic layer depth and limits the phytoplankton growth and consequently prevents the biological uptake of DIP. It resulted in the DIP that mainly showed the characteristic of passive tracer in the river mouth and northwestern offshore region.

The sediment particles could absorb inorganic fractions of nutrients, particularly the DIP, which could inhibit eutrophication in the high-turbidity water, and release the nutrients in the low-turbidity open sea. The previous measurements indicated that 20% of the nutrients are in particulate form in estuarine waters when SPM ~ 10 mg/L. This fraction could be up to ~80% when SPM ~ 1,000 mg/L (Middelburg & Herman, 2007). The background SPM of river mouth is ~400 mg/L (Ge et al., 2020; Ge, Shen, et al., 2015), suggesting that the nutrient-absorbed nutrients could be a significant fraction (Xu et al., 2013). Additionally, the sediment-

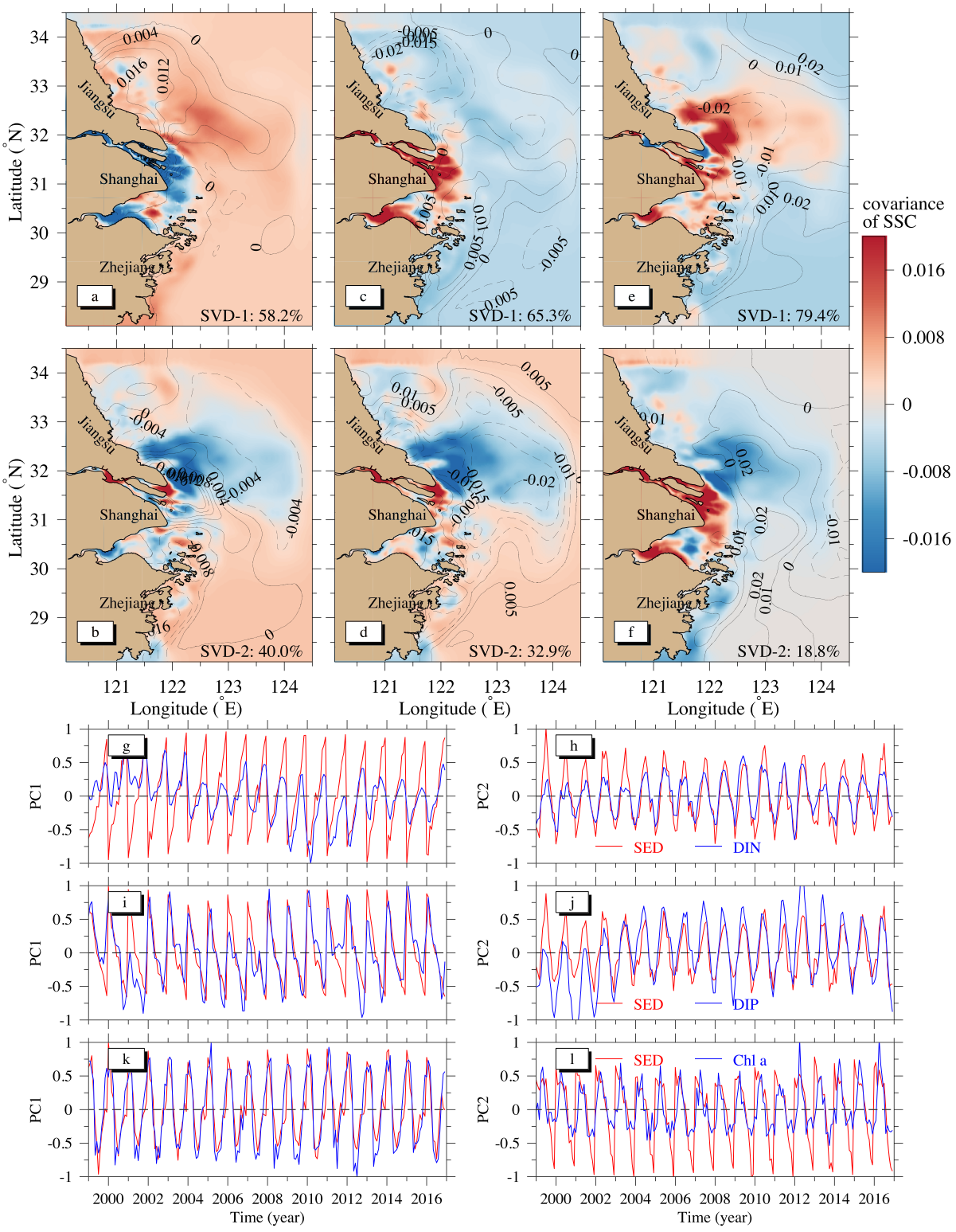

Figure 9. Heterogeneous spatial correlation map of SSC (image) and DIN (contours) for the first (a) and second (b) modes from SVD analysis. First (c) and second (d) modes for paired SSC (image) and DIP (contours), as well as first (e) and second (f) modes for paired SSC (image) and *Chl a* (contours). Their temporal expansion coefficients were also included for the first and second modes for paired SSC and DIN (g, h), SSC and DIP (i, j), and SSC and *Chl a* (k, l).

induced nutrient absorption/desorption is a rapid process (Fitzsimons et al., 2011). If the absorption/desorption is included in the future model simulation, the temporal variabilities will not be notably changed; however, the spatial structure of SVD (SED, DIP) could be significantly altered.

The first mode of SVD (SED, CHL) accounted for most of the variance, reaching 79.4%. The sediment shields mainly covered the river mouth, Hangzhou Bay, and the offshore of Jiangsu. The light penetration free zone was located in the offshore region (Figure 9e). In this area local sediment resuspension was relatively weak due to the tidal current, and the waves applied a relatively small bottom shear stress to erode bed sediment which was entrained in the upper column (Ge, Shen, et al., 2015). The leading two principle components of SVD (SED, CHL) showed high negative correlation between sediment and phytoplankton (Figures 9e and 9f). Seasonal variation was the major component from 1999 to 2016, with interannual variation being relatively weak. The variation in sediment and phytoplankton growth had a moderate correlation of 0.56 (Table 1).

The expansion coefficients of the first modes of SVD (SED, DIN), SVD (SED, DIP), and SVD (SED, CHL) indicated that the suspended sediment concentration showed large seasonal fluctuation with a stable amplitude (Figures 9g, 9i, and 9k). The seasonal timescale was also significant for the second modes, with relatively stable annual cycles (Figures 9h, 9j, and 9l). This pattern indicates that although the concentration of sediment carried by river experienced a decline from 1999 to 2009 and then remained stable until 2016 (Figure 2c), it did not strongly influence the sediment concentration in the estuary. Sediment concentration in the estuary matched the sediment dynamics of the offshore region, which were mainly determined by local resuspension and settling, instead of the river-sourced sediment concentration. It was possible that much longer timescales were required for the decline in riverine sediment concentration to significantly affect the shore sediment front. Around the Zhejiang offshore where the CDW has strong influence and sediment dynamics are weak, the riverine source of freshwater discharge and sediment had weak contribution; thus, the local physical and biological dynamics play the major role in the ecosystem.

6. Variability in Phytoplankton

6.1. Monthly Mean Variability in *Chl a*

Three typical sites located at a longitude of 123°E were selected to determine the variability of phytoplankton within the Zhejiang, Shanghai, and Jiangsu offshore regions (Figure 1b). These sites represented three major water bodies under the influence of the CR. Site 1 is located in the north of the region, and it is under the joint effects of the Yellow Sea Coastal Current and diluted Changjiang water, leading to relatively cold water around Site 3. In contrast, it is under the influence of the Taiwan Warm Current and diluted Changjiang water (Chen et al., 2003), so the surrounding water was relatively warm. Site 2, in the central position where diluted Changjiang water dominates, had an intermediate temperature between Sites 1 and 3.

The different physical conditions in the three water bodies resulted in different patterns of monthly averaged concentrations of phytoplankton *Chl a* (Figure 10). If we define the phytoplankton bloom when *Chl a* concentration is $\geq$5.0 μg/L, the results of the Site 1 analysis demonstrated that spring phytoplankton blooms in the Jiangsu offshore area (Site 1) mainly occurred in May. Overall, the frequency of phytoplankton blooms occurred at Site 1 was much lower than that at the other two sites. The monthly mean *Chl a* concentration only reached $\geq$5.0 μg/L in May of 2012 and 2013 at Site 1. The phytoplankton population showed significant decrease from May to September in the Jiangsu offshore area.

Significant growth of phytoplankton was observed to occur from March to October at Site 2 in the area offshore of Shanghai. The bloom usually began in May, but there were some exceptions that some blooms initiated from April of 2002, 2005, 2012, and 2016. The duration of the bloom significantly increased from 2012 to 2016. The maximum duration of the phytoplankton bloom lasted for 4 months from March to July in both 2012 and 2016.

In the region offshore of Zhejiang (Site 3), the lowest monthly mean *Chl a* concentration was about 2.0 μg/L, and most of the monthly means were larger than 3.0 μg/L. The peak timing of the spring bloom had shifted to early March and April at this location. For the last 18 years, this location had experienced a 2-month spring bloom in most calendar years.

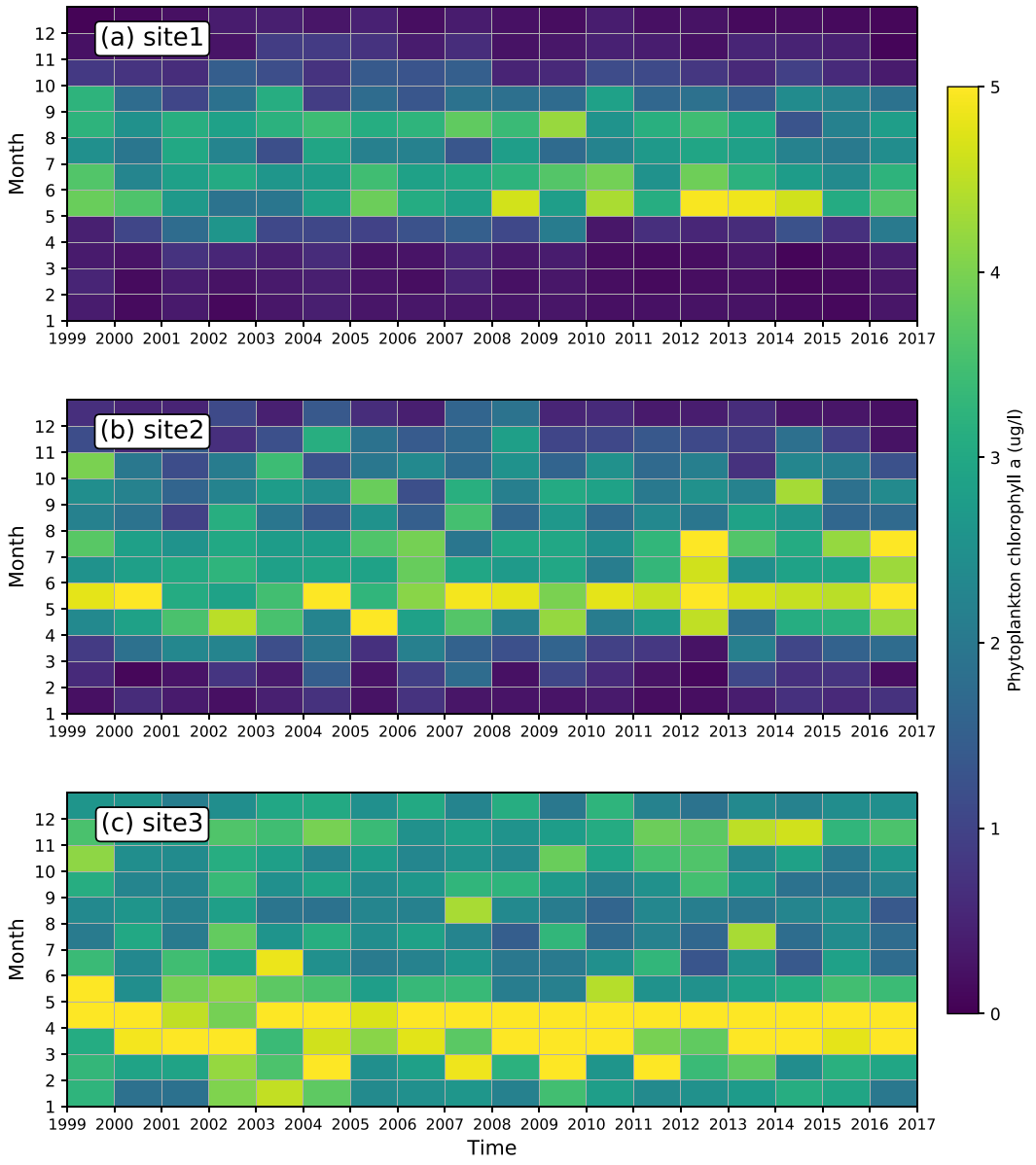

Figure 10. Monthly mean concentration of *Chl a* at Sites 1, 2, and 3 from 1999 to 2016.

6.2. Ratios of Diatom and Dinoflagellate Species

Chl a does not reflect the concentration of specific phytoplankton species or total phytoplankton biomass. Therefore, the carbon concentration of four specific phytoplankton function groups (picophytoplankton, nanophytoplankton, microphytoplankton, and diatoms) was used to represent their own biomass. According to the classification of these function groups based on the single trait size in ERSEM model, the microphytoplankton could be recognized as dinoflagellate group as its averaged trait size is less than that of diatom but >20 μm.

The model demonstrated strong seasonal and interannual variations in the diatom/dinoflagellate ratio (Figure 11). In the wintertime, diatoms were the dominant species in the phytoplankton community. The ratio reached 1.8 at Site 1, 2.4 at Site 2, and 2.3 at Site 3. The ratio peak at Site 3 could be observed to have about a 1 month delay compared with Site 1. However, this ratio dropped below 0.6 for all three sites during summer, indicating that the dinoflagellate became the dominant phytoplankton species at all sites in the

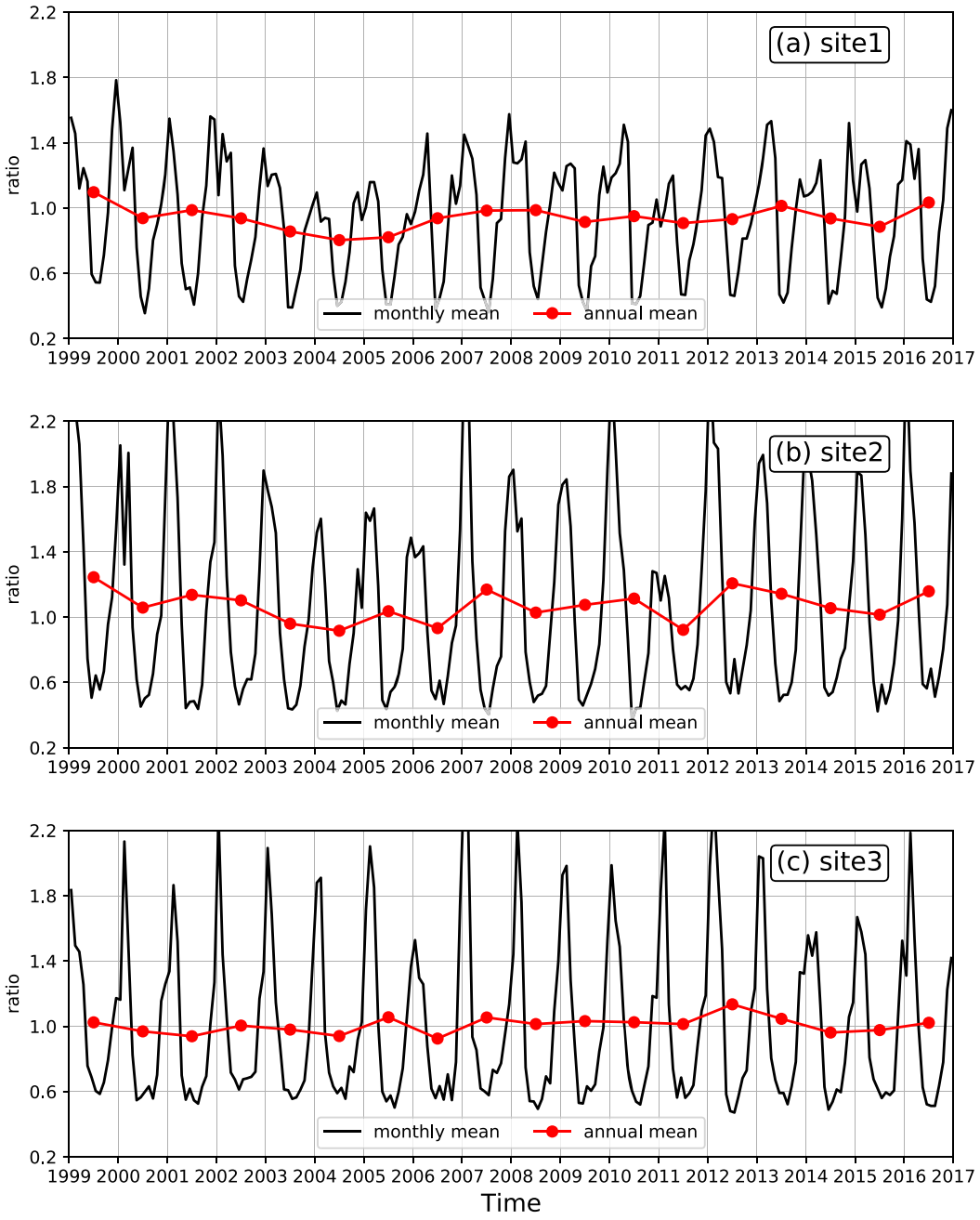

Figure 11. Time series of monthly and annual biomass ratio between diatom and dinoflagellate at Site 1, 2 and 3.

Changjiang offshore region. For the Jiangsu offshore region, this ratio could reach up to 0.4 in the summertime.

The ratio of diatom to dinoflagellate had maxima during winter. At that time, the dissolved inorganic nutrients in the water column were adequate for the growth of both diatoms and dinoflagellates. The limiting influences likely came from the physical factors solar radiation, deep water mixing, and temperature. The coupled model outputs revealed the spatial and temporal variations of water temperature and found that the water temperature from the previous December to February in 2011, 2012, and 2016 and other years with ratio >2.2 at Site 3 were all higher (Figure 11c). It caused relatively strong growth of diatom in corresponding January and February, producing high ratios.

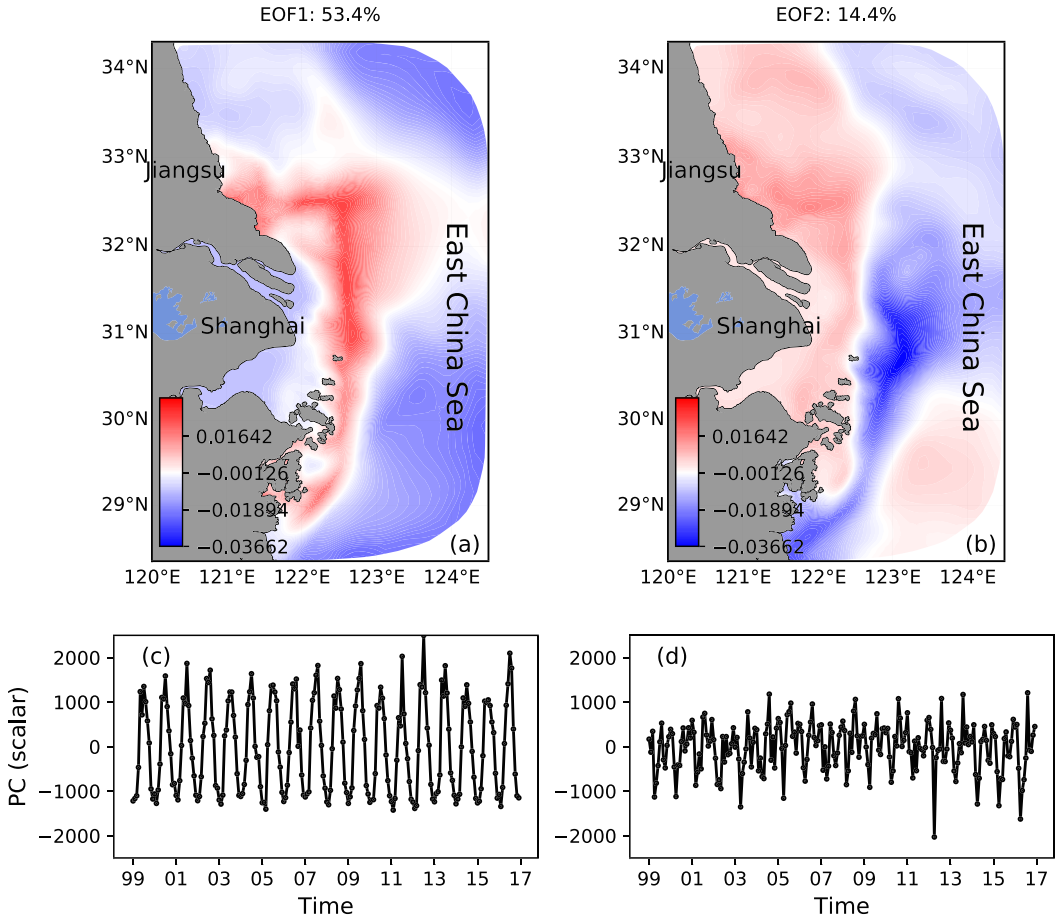

Figure 12. Spatial structure of first (a) and second (b) EOF modes of diatom primary production. The lower panels show corresponding time series (dimensionless scalar) of principle components of first (c) and second (d) modes.

Most of the annual mean ratios remained below 1.0 at Site 1 over the last 18 years, suggesting that dinoflagellate not only dominated during summertime at this location but also remained the major species throughout the entire year. This pattern was not reflected offshore of Shanghai and Zhejiang. The annual mean ratios at these two sites had small fluctuations around 1.0.

During the annual phytoplankton bloom which occurred from March to June across the entire study region (Figure 9), the diatom/dinoflagellate ratios were always around 0.6. This suggested that the dinoflagellate was consistently the major biomass contributor during the spring bloom.

Interannual variation in the diatom/dinoflagellate ratio can also be determined in the 18 year simulation. All three sites had experienced a ratio drop from 2003, which reached a low value in 2006; this could be related to the negative anomaly observed in river discharge from 2003 to 2006 (Figure 6a). Another significant ratio decreases at all three sites occurred in 2010–2011, corresponding to another negative discharge anomaly at the same time period. The nutrient source at the Datong station also measured a strong decline in nitrate, phosphate, and ammonia concentration at the end of 2010. This indicated that the ecosystem has quick response to the river's variations of both discharge rate and nutrient concentration.

6.3. Variability in Diatom and Dinoflagellate Populations

To determine the spatial pattern and temporal evolution of phytoplankton production, an EOF analysis for primary production of diatoms and dinoflagellates, which are two major phytoplankton groups, was conducted. The EOF results demonstrated that the spatial variability in diatom primary production was well revealed by the first and second modes, which represents 53.4% and 14.4% of the total variance, respectively (Figures 12a and 12b). Mode 1 (Figure 12a) represented the offshore sediment front region from the Jiangsu

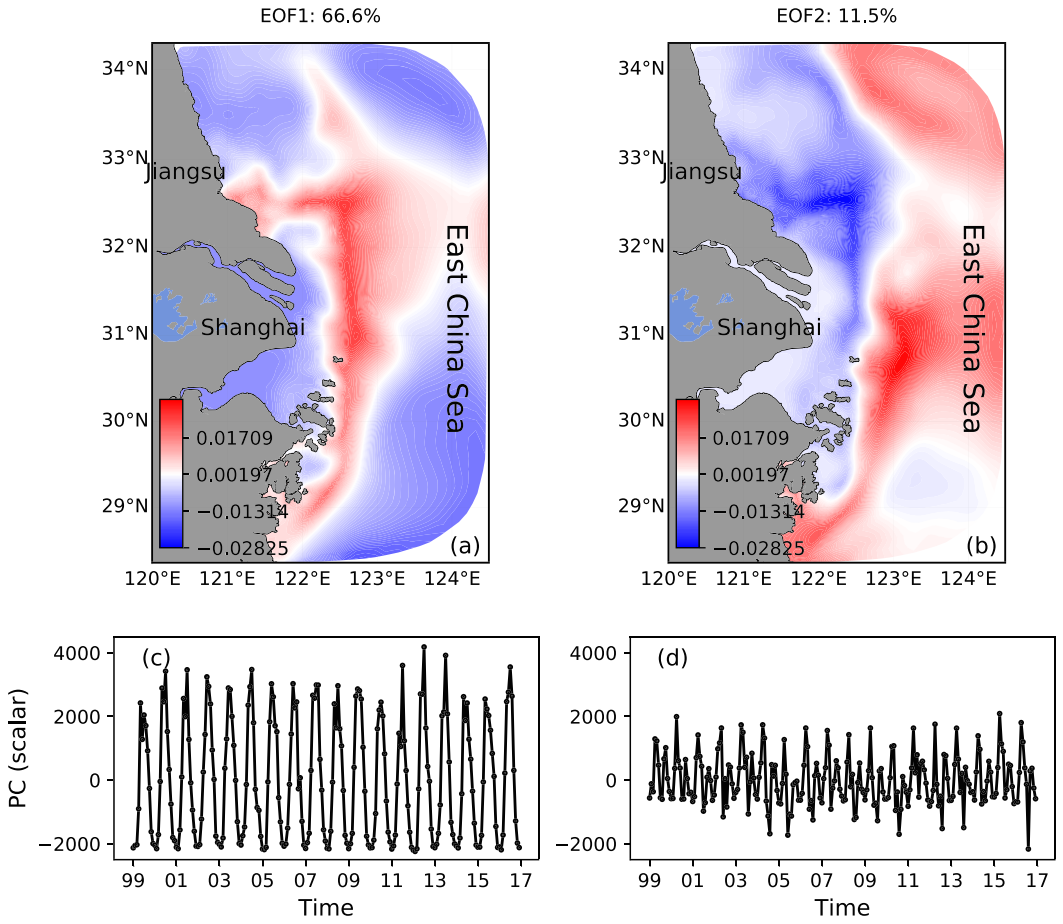

Figure 13. Spatial structure of first (a) and second (b) EOF modes of dinoflagellate primary production. The lower panels show corresponding time series (dimensionless scalar) of principle components of first (c) and second (d) modes.

coast to offshore Zhejiang. The offshore sediment front was a boundary where, to the east sediment, concentration was low, producing a region for improved light penetration. The Mode 1 amplitude from time series analysis indicated high values of principle component from early spring to autumn and low values from late autumn to winter (Figure 12c). This pattern was similar to the spatial structure of *Chl a* concentration (Figure 9e), which indicated that the spatial pattern of diatom primary production was mainly controlled by sediment dispersion and suspension.

Mode 2 of diatom primary production represented the offshore deeper region, where the bathymetry was >30 m (Figure 12b). This was a transitional region from the sediment front to an outer ocean circulation controlled region. The principal component of Mode 2 had low values in the spring (Figure 12d) corresponding with the spring diatom bloom.

The spatial variability in dinoflagellate primary production was also split into two major modes through EOF analysis. The first and second modes accounted for 66.6% and 11.5% of the total variance, respectively. The spatial pattern of dinoflagellate primary production was similar to that of the diatom (Figure 13a). The distribution also indicated the impact of sediment on the growth of dinoflagellate. However, the spatial variability observed in dinoflagellate primary production was not only preserved along the sediment front but also extended offshore into the northeastern region (Figure 13a), suggesting that the dinoflagellate had significant dominance in the offshore region. The principle component of Mode 1 had corresponding high values from spring to autumn (Figure 13c), which corresponded to high values in dinoflagellate biomass at that time (Figure 11).

Mode 2 of dinoflagellate primary production showed high values in the offshore deep region (Figure 13b), outside of the sediment front, which suggested that the dinoflagellates were experiencing active growth in the offshore region. The amplitude from Mode 2 time series analysis showed peak values in spring corresponding with major bloom occurrences and secondary peaks in autumn coinciding with a dinoflagellate-induced autumn bloom (Figure 13d).

7. Conclusions

A coupled physical-biogeochemical model system coupling FVCOM and ERSEM through the framework of FABM was developed to examine the seasonal and interannual variability of coastal nutrients and phytoplankton dynamics during 1999–2016 in the high-turbidity Changjiang Estuary. Model outputs revealed a clear ecosystem response to the fluvial contributions of freshwater, nutrients, and sediment load. The regional total nutrient budget, including nitrogen, phosphorus, and silicate, had similar variation patterns to river discharge, indicating that the CR is a major nutrient source for the nearshore and offshore regions in that area. SVD analysis indicated that nitrate supply from the river experienced a dilution process in the nearshore region. However, phosphate was not fully related to advective transport during river-to-shelf continuum, but mainly local physical and biological dynamics in the offshore regions, which was coherent with phytoplankton-induced consumption and vertical mixing. Sediment particulate dispersion did not directly change the temporal variability of dissolved nutrients. But the sediments controlled the phytoplankton production and thus the nutrient variability. It should be noted that this study has only looked at dissolved inorganic nutrients, and future studies should include the advection of organic or particulate nutrients from fluvial, coastal, and oceanic sources.

The spatial variability in *Chl a*, on the other hand, coincided with variation in the sediment front. Phytoplankton had a longer bloom duration and higher *Chl a* concentration offshore of Zhejiang, and they both decreased in Shanghai and Jiangsu offshore regions. Quantification of the monthly and annual diatom and dinoflagellate biomass indicated that the dinoflagellates had become the dominant species in the phytoplankton community. The diatom/dinoflagellate ratio reaches below 0.6 for all selected sites during the phytoplankton bloom.

The phytoplankton population responded rapidly to the shifting river impact. The interannual variability in the phytoplankton species ratio matched well with a negative anomaly in river discharge from 2003 to 2006, and it also coincided with a significant decline in nutrient concentration at the end of 2010.

Our model has determined the different spatial and temporal ecosystem functionalities of both diatoms and dinoflagellates. The primary production of diatoms was distributed near the sediment front. In contrast, dinoflagellate primary production extended significantly offshore into the deep ocean. Both diatom and dinoflagellate populations had major peaks that represented spring blooms in the time series analysis of the principle components of EOF Modes 1 and 2 and secondary peaks from Mode 2 in the autumn, which coincided with the autumn bloom.

Acknowledgments

J. Ge, S. Shi, P. Ding, and Y. Xu were supported by the National Key R&D Program of China (Grant 2016YFA0600903) and the National Natural Science Foundation of China (Grants 41776104, 41761144062, and 41606025). R. Bellerby was supported by the National Thousand Talents Program for Foreign Experts 294 (Grant WQ20133100150), the Vulnerabilities and Opportunities of the Coastal Ocean (Grant 295 SKLEC-2016RCDW01), Marginal Seas (MARSEAS) (Grant SKLEC-Task-team project), and the NIVA Land-Ocean 299 Interactions Strategic Institute program. J. Liu was supported by the China Scholarship Council-201913045. Authors appreciated the help from Weiqi Li and Jianfei Ma for collecting historical data, including the nutrients, *Chl a*, and riverine data set. Professors Zhijun Dai and Zhuoyi Zhu kindly provided historical nutrients data. All data sets and model results used in this study are public available online (https://figshare.com/s/ab600431c5958ee9d261). Authors also would like to thank three anonymous reviewers for providing constructive comments and suggestions on the manuscript.

References

Bianchi, T. S., Engelhaupt, E., Westman, P., Andrén, T., Rolff, C., & Elmgren, R. (2000). Cyanobacterial blooms in the Baltic Sea: Natural or human-induced? *Limnology and Oceanography*, *45*(3), 716–726. http://doi.org/10.4319/lo.2000.45.3.0716

Bjornsson, H., Venegas, S.A. (1997). A manual for EOF and SVD analyses of climate data. Department of Atmospheric and Oceanic Sciences and Center of Climate and Global Change Research, McGill University.

Bruggeman, J., & Bolding, K. (2014). A general framework for aquatic biogeochemical models. *Environmental Modelling and Software*, *61*(C), 249–265. http://doi.org/10.1016/j.envsoft.2014.04.002

Butenschön, M., Clark, J., Aldridge, J. N., Allen, J. I., Artioli, Y., Blackford, J., et al. (2016). ERSEM 15.06: A generic model for marine biogeochemistry and the ecosystem dynamics of the lower trophic levels. *Geoscientific Model Development*, *9*(4), 1293–1339. http://doi.org/10.5194/gmd-9-1293-2016-supplement

Chen, C., Xue, P., Ding, P., Beardsley, R. C., Xu, Q., Mao, X., et al. (2008). Physical mechanisms for the offshore detachment of the Changjiang diluted water in the East China Sea. *Journal of Geophysical Research*, *113*, C02002. http://doi.org/10.1029/2006JC003994

Chen, C., Zhu, J., Beardsley, R. C., & Franks, P. J. S. (2003). Physical-biological sources for dense algal blooms near the Changjiang River. *Geophysical Research Letters*, *30*(10), 1515. http://doi.org/10.1029/2002GL016391

Chetelat, B., Liu, C. Q., Zhao, Z. Q., Wang, Q. L., Li, S. L., Li, J., & Wang, B. L. (2008). Geochemistry of the dissolved load of the Changjiang Basin rivers: Anthropogenic impacts and chemical weathering. *Geochimica et Cosmochimica Acta*, *72*, 4254–4277. https://doi.org/10.1016/j.gca.2008.06.013

CWRC (Changjiang Water Resources Commission) (2011). Changjiang sediment bulletin. available at: http://www.cjw.gov.cn/zwzc/bmgb/ (in Chinese).

Dai, Z., Du, J., Zhang, X., Su, N., & Li, J. (2011). Variation of riverine material loads and environmental consequences on the Changjiang (Yangtze) estuary in recent decades (1955–2008). *Environmental Science and Technology*, *45*(1), 223–227. http://doi.org/10.1021/es103026a

Fitzsimons, M. F., Lohan, M. C., Tappin, A. D., & Millward, G. E. (2011). The role of suspended particles in estuarine and coastal biogeochemistry. In *Treatise on Estuarine and Coastal Science*, (Vol. 4, pp. 71–114). Amsterdam: Elsevier.

Gaillardet, J., Dupré, B., & Allègre, C. J. (1999). Geochemistry of large river suspended sediments: Silicate weathering or recycling tracer? *Geochimica et Cosmochimica Acta*, *63*, 4037–4051. https://doi.org/10.1016/S0016-7037(99)00307-5

Gao, L., Li, D., & Zhang, Y. (2012). Nutrients and particulate organic matter discharged by the Changjiang (Yangtze River): Seasonal variations and temporal trends. *Journal of Geophysical Research*, *117*, G04001. http://doi.org/10.1029/2012JG001952

Ge, J., Ding, P., & Chen, C. (2015). Low-salinity plume detachment under non-uniform summer wind off the Changjiang Estuary. *Estuarine, Coastal and Shelf Science*, *156*(C), 61–70. http://doi.org/10.1016/j.ecss.2014.10.012

Ge, J., Ding, P., Chen, C., Hu, S., Fu, G., & Wu, L. (2013). An integrated East China Sea–Changjiang Estuary model system with aim at resolving multi-scale regional–shelf–estuarine dynamics. *Ocean Dynamics*, *63*(8), 881–900. http://doi.org/10.1007/s10236-013-0631-3

Ge, J., Shen, F., Guo, W., Chen, C., & Ding, P. (2015). Estimation of critical shear stress for erosion in the Changjiang Estuary: A synergy research of observation, GOCI sensing and modeling. *Journal of Geophysical Research: Oceans*, *120*, 8439–8465. http://doi.org/10.1002/2015JC010992

Ge, J., Torres, R., Chen, C., Liu, J., Xu, Y., Bellerby, R., et al. (2020). Influence of suspended sediment front on nutrients and phytoplankton dynamics off the Changjiang Estuary: A FVCOM-ERSEM coupled model experiment. *Journal of Marine Systems*, *204*, 103292. http://doi.org/10.1016/j.jmarsys.2019.103292

Giosan, L., Syvitski, J., Constantinescu, S., & Day, J. (2014). Climate change: Protect the world's deltas. *Nature*, *516*(7529), 31–33. https://doi.org/10.1038/516031a

Hou, X., Dong, Q., Xue, C., & Wu, S. (2016). Seasonal and interannual variability of chlorophyll-a and associated physical synchronous variability in the western tropical Pacific. *Journal of Marine Systems*, *158*(C), 59–71. http://doi.org/10.1016/j.jmarsys.2016.01.008

Jiang, T., Yu, Z., Song, X., Cao, X., & Yuan, Y. (2010). Long-term ecological interactions between nutrient and phytoplankton community in the Changjiang estuary. *Chinese Journal of Oceanology and Limnology*, *28*(4), 887–898. http://doi.org/10.1007/s00343-010-9059-5

Li, M., Lee, Y. J., Testa, J. M., Li, Y., Ni, W., Kemp, W. M., & Di Toro, D. M. (2016). What drives interannual variability of hypoxia in Chesapeake Bay: Climate forcing versus nutrient loading? *Geophysical Research Letters*, *43*, 2127–2134. https://doi.org/10.1002/2015GL067334

Li, M., Xu, K., Watanabe, M., & Chen, Z. (2007). Long-term variations in dissolved silicate, nitrogen, and phosphorus flux from the Yangtze River into the East China Sea and impacts on estuarine ecosystem. *Estuarine, Coastal and Shelf Science*, *71*(1-2), 3–12. http://doi.org/10.1016/j.ecss.2006.08.013

Lou, X., & Hu, C. (2014). Diurnal changes of a harmful algal bloom in the East China Sea: Observations from GOCI. *Remote Sensing of Environment*, *140*, 562–572. http://doi.org/10.1016/j.rse.2013.09.031

Luan, H. L., Ding, P. X., Wang, Z. B., Ge, J. Z., & Yang, S. L. (2016). Decadal morphological evolution of the Yangtze Estuary in response to river input changes and estuarine engineering projects. *Geomorphology*, *265*(C), 12–23. http://doi.org/10.1016/j.geomorph.2016.04.022

Mackenzie, F. T., Ver, L. M., & Lerman, A. (2002). Century-scale nitrogen and phosphorus controls of the carbon cycle. *Chemical Geology*, *190*(1-4), 13–32. http://doi.org/10.1016/S0009-2541(02)00108-0

Middelburg, J. J., & Herman, P. M. J. (2007). Organic matter processing in tidal estuaries. *Marine Chemistry*, *106*(1-2), 127–147. http://doi.org/10.1016/j.marchem.2006.02.007

Milliman, J. D., & Farnsworth, K. L. (2011). *River discharge to the coastal ocean: A global synthesis*. Cambridge: Cambridge University Press.

Oviatt, C., Smith, L., Krumholz, J., Coupland, C., Stoffel, H., Keller, A., et al. (2017). Managed nutrient reduction impacts on nutrient concentrations, water clarity, primary production, and hypoxia in a north temperate estuary. *Estuarine, Coastal and Shelf Science*, *199*, 25–34. http://doi.org/10.1016/j.ecss.2017.09.026

Qi, J., Chen, C., Beardsley, R. C., Perrie, W., Cowles, G. W., & Lai, Z. (2009). An unstructured-grid finite-volume surface wave model (FVCOM-SWAVE): Implementation, validations and applications. *Ocean Modelling*, *28*(1-3), 153–166. http://doi.org/10.1016/j.ocemod.2009.01.007

Ragueneau, O., Conley, D. J., Leynaert, A., Longphuirt, S. N., & Slomp, C. P. (2006). Responses of coastal ecosystems to anthropogenic perturbations of silicon cycling. In V. Ittekot, D. Unger, C. Humborg, & N. A. An (Eds.), *The silicon cycle*, (pp. 197–214). Washington: Island press.

Ram, A., Jaiswar, J. R. M., Rokade, M. A., Bharti, S., Vishwasrao, C., & Majithiya, D. (2014). Nutrients, hypoxia and Mass Fishkill events in Tapi Estuary, India. *Estuarine, Coastal and Shelf Science*, *148*(C), 48–58. http://doi.org/10.1016/j.ecss.2014.06.013

Shi, X., Li, H., & Wang, H. (2014). Nutrient structure of the Taiwan Warm Current and estimation of vertical nutrient fluxes in upwelling areas in the East China Sea in summer. *Journal of Ocean University of China*, *13*(4), 613–620. http://doi.org/10.1007/s11802-014-2481-0

Statham, P. J. (2012). Nutrients in estuaries—An overview and the potential impacts of climate change. *Science of the Total Environment*, *434*(C), 213–227. http://doi.org/10.1016/j.scitotenv.2011.09.088

Tian, R., Chen, C., Qi, J., Ji, R., Beardsley, R. C., & Davis, C. (2015). Model study of nutrient and phytoplankton dynamics in the Gulf of Maine: Patterns and drivers for seasonal and interannual variability. *ICES Journal of Marine Science*, *72*(2), 388–402. http://doi.org/10.1093/icesjms/fsu090

Uncles, R., Frickers, P., & Harris, C. (2003). Dissolved nutrients in the Tweed Estuary, UK: Inputs, distributions and effects of residence time. *Science of the Total Environment*, *314-316*, 727–736. http://doi.org/10.1016/S0048-9697(03)00080-9

Wang, B. (2006). Cultural eutrophication in the Changjiang (Yangtze River) plume: History and perspective. *Estuarine, Coastal and Shelf Science*, *69*(3–4), 471–477. https://doi.org/10.1016/j.ecss.2006.05.010

Wang, H., Wu, X., Bi, N., Li, S., Yuan, P., Wang, A., et al. (2017). Impacts of the dam-orientated water-sediment regulation scheme on the lower reaches and delta of the Yellow River (Huanghe). A review. *Global and Planetary Change*, *157*, 93–113. http://doi.org/10.1016/j.gloplacha.2017.08.005

Wang, L., Chen, Q., Han, R., Wang, B., & Tang, X. (2017). Responses of the phytoplankton community in the Yangtze River estuary and adjacent sea areas to the impoundment of the Three Gorges Reservoir. *Annales de Limnologie - International Journal of Limnology*, *53*, 1–10. http://doi.org/10.1051/limn/2016027

Wu, L., Chen, C., Guo, P., Shi, M., Qi, J., & Ge, J. (2011). A FVCOM-based unstructured grid wave, current, sediment transport model. I. Model description and validation. *Journal of Ocean University of China*, *10*(1), 1–8. http://doi.org/10.1007/s11802-011-1788-3

Xu, H., Wolanski, E., & Chen, Z. (2013). Suspended particulate matter affects the nutrient budget of turbid estuaries: Modification of the LOICZ model and application to the Yangtze Estuary. *Estuarine, Coastal and Shelf Science*, *127*(C), 59–62. http://doi.org/10.1016/j.ecss.2013.04.020

Xue, P., Chen, C., Ding, P., Beardsley, R. C., Lin, H., Ge, J., & Kong, Y. (2009). Saltwater intrusion into the Changjiang River: A model-guided mechanism study. *Journal of Geophysical Research-Oceans*, *114*, C02006. https://doi.org/10.1029/2008JC004831

Yang, D., Yin, B., Sun, J., & Zhang, Y. (2013). Numerical study on the origins and the forcing mechanism of the phosphate in upwelling areas off the coast of Zhejiang province, China in summer. *Journal of Marine Systems*, *123-124*(C), 1–18. http://doi.org/10.1016/j.jmarsys.2013.04.002

Yang, S. L., Xu, K. H., Milliman, J. D., Yang, H. F., & Wu, C. S. (2015). Decline of Yangtze River water and sediment discharge: Impact from natural and anthropogenic changes. *Scientific Reports*, *5*(1), 1–14. http://doi.org/10.1038/srep12581

Zhang, J., Wu, Y., Jennerjahn, T. C., Ittekkot, V., & He, Q. (2007). Distribution of organic matter in the Changjiang (Yangtze River) Estuary and their stable carbon and nitrogen isotopic ratios: Implications for source discrimination and sedimentary dynamics. *Marine Chemistry*, *106*(1-2), 111–126. http://doi.org/10.1016/j.marchem.2007.02.003

Zhang, J., Zhang, Z. F., Liu, S. M., Wu, Y., Xiong, H., & Chen, H. T. (1999). Human impacts on the large world rivers: Would the Changjiang (Yangtze River) be an illustration? *Global Biogeochemical Cycles*, *13*(4), 1099–1105. http://doi.org/10.1029/1999GB900044

Zhou, M. J., Shen, Z. L., & Yu, R. C. (2008). Responses of a coastal phytoplankton community to increased nutrient input from the Changjiang (Yangtze) River. *Continental Shelf Research*, *28*(12), 1483–1489. http://doi.org/10.1016/j.csr.2007.02.009

Zhou, Z. X., Yu, R. C., & Zhou, M. J. (2017). Resolving the complex relationship between harmful algal blooms and environmental factors in the coastal waters adjacent to the Changjiang River estuary. *Harmful Algae*, *62*, 60–72. http://doi.org/10.1016/j.hal.2016.12.006

Zhu, Z. Y., Ng, W. M., Liu, S. M., Zhang, J., Chen, J. C., & Wu, Y. (2009). Estuarine phytoplankton dynamics and shift of limiting factors: A study in the Changjiang (Yangtze River) Estuary and adjacent area. *Estuarine, Coastal and Shelf Science*, *84*(3), 393–401. http://doi.org/10.1016/j.ecss.2009.07.005

Zhu, Z. Y., Wu, Y., Zhang, J., Du, J. Z., & Zhang, G. S. (2014). Reconstruction of anthropogenic eutrophication in the region off the Changjiang Estuary and central Yellow Sea from decades to centuries. *Continental Shelf Research*, *72*(C), 152–162. http://doi.org/10.1016/j.csr.2013.10.018